

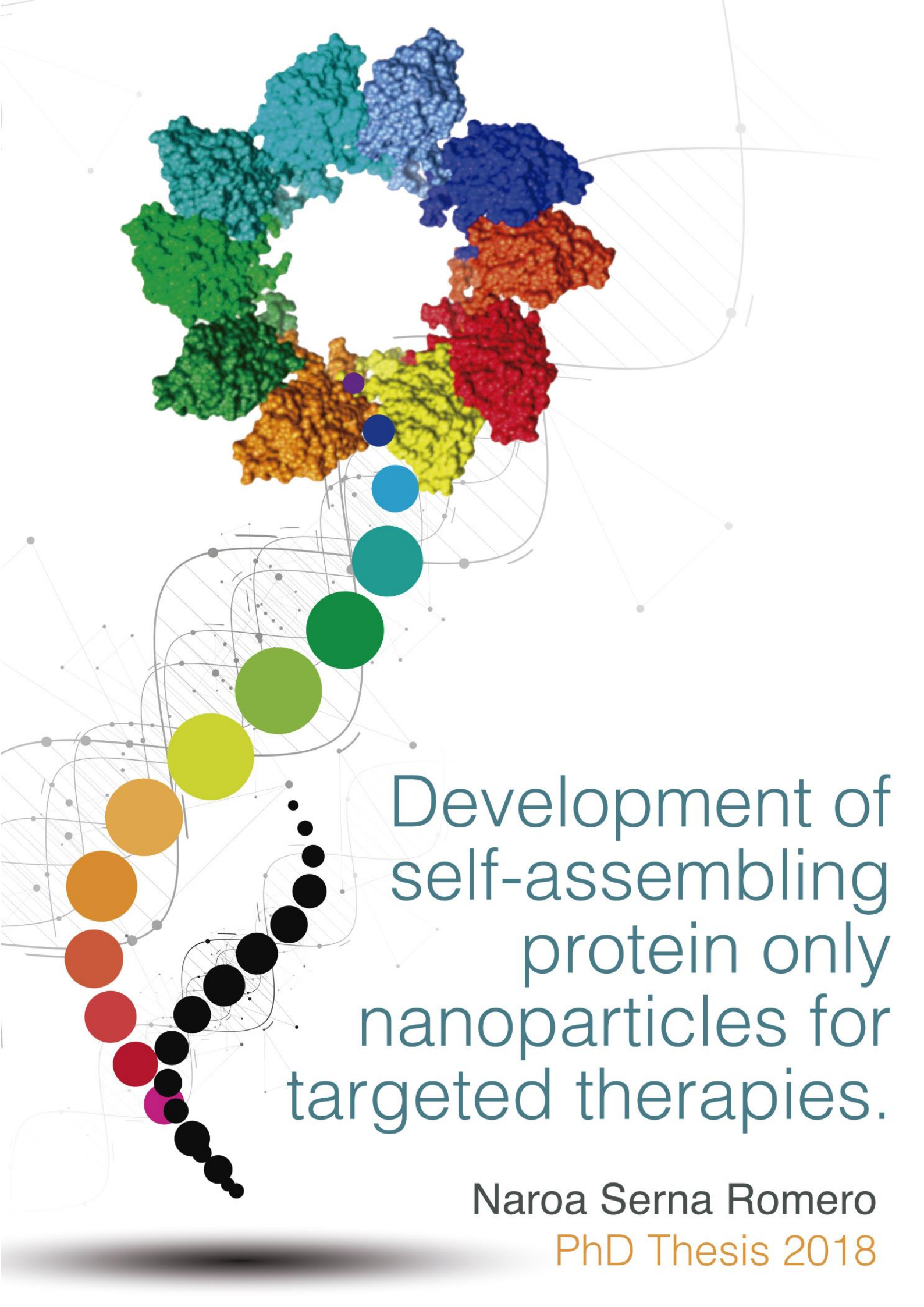


Universitat Autònoma de Barcelona

**ADVERTIMENT.** L'accés als continguts d'aquesta tesi queda condicionat a l'acceptació de les condicions d'ús establertes per la següent llicència Creative Commons:  [http://cat.creativecommons.org/?page\\_id=184](http://cat.creativecommons.org/?page_id=184)

**ADVERTENCIA.** El acceso a los contenidos de esta tesis queda condicionado a la aceptación de las condiciones de uso establecidas por la siguiente licencia Creative Commons:  <http://es.creativecommons.org/blog/licencias/>

**WARNING.** The access to the contents of this doctoral thesis it is limited to the acceptance of the use conditions set by the following Creative Commons license:  <https://creativecommons.org/licenses/?lang=en>



Development of  
self-assembling  
protein only  
nanoparticles for  
targeted therapies.

Naroa Serna Romero  
PhD Thesis 2018



Doctorat en Biotecnologia

# DEVELOPMENT OF SELF-ASSEMBLING PROTEIN ONLY NANOPARTICLES FOR TARGETED THERAPIES.

Tesi doctoral – 2018

Departament de Genètica i de Microbiologia –  
Facultat de Biociències



Memòria presentada per Naroa Serna Romero per optar al grau de doctor en Biotecnologia per la Universitat Autònoma de Barcelona.

Naroa Serna Romero

Vist i plau dels directors de la tesis:

Antonio Villaverde Corrales

Ugutx Unzueta Elorza

Neus Ferrer-Miralles

Aquest treball ha estat realitzat principalment al Institut de Biotecnologia i de Biomedicina, Vicent Villar I Palasí, sota la direcció dels doctors Antonio Villaverde Corrales, Ugutz Unzueta Elorza i Neus Ferrer-Miralles. Una part, però, s'ha dut a terme al Centre Mèdic Acadèmic d' Amsterdam, Holanda.





**A todos aquellos que me han apoyado durante la tesis,**

**Tesia egiterakoan lagundu nauzuen guztiei,**

**A tots aquells que *m'han* ajudat durant la tesi,**

**To all those who have supported me during my thesis,**





# CONTENTS



<b>CONTENTS</b> .....	<b>1</b>
<b>INTRODUCTION</b> .....	<b>5</b>
<b>1. NANOMEDICINE: THERAPEUTIC NANOPARTICLES</b> .....	<b>7</b>
1.1. TARGETING STRATEGY.....	8
1.2. PHYSICOCHEMICAL PROPERTIES OF NANOPARTICLES.....	10
1.3. BIOCOMPATIBILITY.....	15
<b>2. APPLICATIONS OF THERAPEUTIC NANOPARTICLES</b> .....	<b>16</b>
2.1. ONCOLOGY.....	16
2.2. INFECTIOUS DISEASES.....	21
2.3. CENTRAL NERVOUS SYSTEM DISEASES.....	24
<b>3. PROTEIN-BASED NANOPARTICLES</b> .....	<b>27</b>
3.1. DRUG-LOADED PROTEIN NANOPARTICLES.....	27
3.2. PROTEIN ONLY NANOPARTICLES: CYTOTOXIC PROTEINS AS DRUGS.....	37
<b>4. OVERVIEW</b> .....	<b>39</b>
<b>OBJECTIVES</b> .....	<b>41</b>
<b>RESULTS</b> .....	<b>45</b>
<b>ARTICLE 1</b> .....	<b>47</b>
<b>ARTICLE 2</b> .....	<b>61</b>
<b>ARTICLE 3</b> .....	<b>73</b>
<b>REVIEW 1</b> .....	<b>83</b>
<b>DISCUSSION</b> .....	<b>113</b>
<b>CONCLUSIONS</b> .....	<b>133</b>
<b>REFERENCES</b> .....	<b>137</b>
<b>ANNEXES</b> .....	<b>165</b>
<b>ANNEX 1: ARTICLE 4</b> .....	<b>167</b>
<b>ANNEX 2: DRAFT 1</b> .....	<b>181</b>
<b>ANNEX 3: ARTICLE 5</b> .....	<b>203</b>
<b>ANNEX 4: MANUSCRIPT 1</b> .....	<b>209</b>
<b>ANNEX 5: MANUSCRIPT 2</b> .....	<b>229</b>
<b>ANNEX 6: REFERENCE 295</b> .....	<b>257</b>
<b>ANNEX 7: EUROPEAN PATENT</b> .....	<b>269</b>
<b>ACKNOWLEDGEMENTS</b> .....	<b>277</b>







# INTRODUCTION





## 1. NANOMEDICINE: THERAPEUTIC NANOPARTICLES.

The term “nano-technology” was initially introduced to refer to the development and handling of small-scale applicative materials (1 to 100 nm)<sup>1;2</sup>. This is currently a field of intense scientific research with potential applications in a variety of areas such as medicine, optics and electronics. Nanomedicine is the application of nanotechnology to medicine<sup>3</sup>.

Nanomedicine involves any medical application of nanoscale materials, compounds or technologies for diagnosis, delivery or sensing. The European Science Foundation highlights five key disciplines of nanomedicine<sup>4</sup>: 1) analytical tools 2) nanoimaging 3) nanomaterials and nanodevices 4) novel therapeutics and drug delivery systems and 5) clinical, regulatory, and toxicological issues. One of the most currently promising approaches within nanomedicines is the targeted drug delivery (Figure 1).

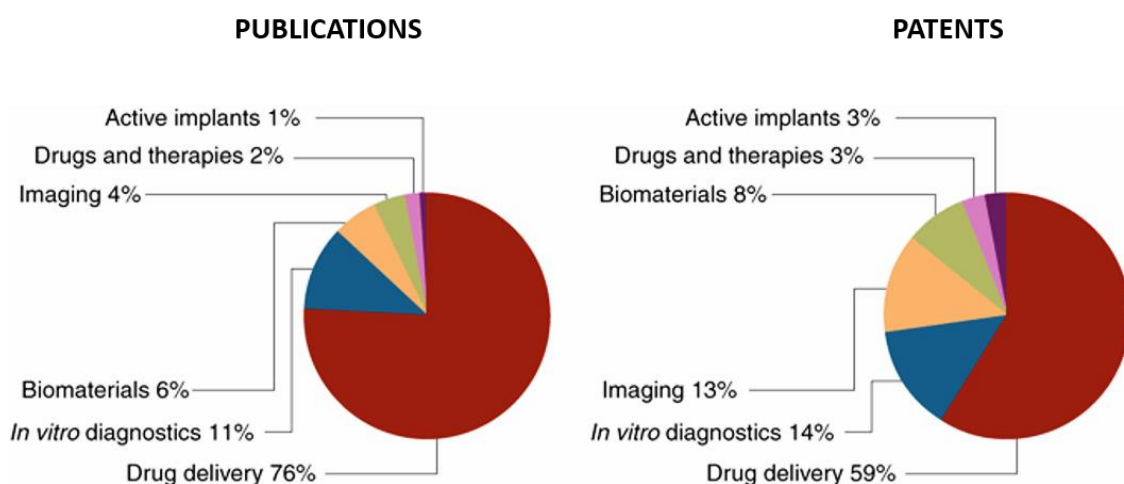


*Figure 1:* Sectorial breakdown of Nanomedicine. Modified from <sup>1</sup>.

**Drug delivery systems (DDS)** are engineered nanoscale platforms for the targeted delivery and controlled release of therapeutic agents<sup>5;6</sup>. Understanding the physiological barriers to efficient drug delivery is a pivotal matter, such as the transport in the circulatory system and drug movement through cells and tissues<sup>7</sup>. There are a variety of modes of drug delivery that have entered clinical practice<sup>8</sup>. However, many drug delivery devices, even those discovered using the most advanced molecular biology strategies such as liposomes, micelles, dendrimers, hydrogels and

nano-crystals, among others, have unacceptable side effects due to the drug interacting with off-target healthy tissues and its poor biodegradability<sup>9</sup>. Therefore, new nanomedical approaches for targeted drug delivery are aimed to develop smart nanosized cages or nanoparticles (NPs) with high stability, specificity, biocompatibility, appropriate pharmacokinetics and efficient cell penetrability<sup>10;11</sup>. In other words, any DDS should recruit a set of biological activities that empower it with appropriate biodistribution and therefore, the capacity to deliver the cargo material into the appropriate compartment of target cells leading to an enhanced efficacy and reduced toxicity.

### 1.1. TARGETING STRATEGY.

Conventional therapies for many diseases are mainly based on systemically administered drugs such as chemotherapeutics for cancer or antibiotics for infections. The insufficient therapeutic effect of these drugs is related to their small molecular size, that being below renal filtration cut-off (around 6 nm)<sup>7</sup> are excreted through the kidney, what results in a short circulation time.

The coupling of these drugs to a vehicle allows the nanoscale size of the drug enabling them to escape renal clearance, rendering them long plasma half-life and therefore, favouring the enhanced permeability and retention effect (EPR)<sup>12;13</sup>. This effect is based on the selective extravasation and accumulation of these compounds in target tissue due to its hypervascularization. This targeting strategy is known as **passive targeting** and the majority of nanostructured drugs that have reached clinics are based on it<sup>14;15</sup>. The first vehicles used to enhance the half-life in plasma of carried drugs were mainly based on liposomes and polymer–drug conjugates that enhanced their deposition in target tissues. Since their approval, many other liposome/polymer-based vehicles have been approved for oncology, fungal infections, cardiovascular diseases, hepatitis and neutropaenia among other diseases.

Currently available platforms, lacking specificity, offer only limited improvements over conventional formulations and patient responses remain still modest. Indeed, the amount of drug that reaches target cells remains low and is not sufficient to ensure a maximal reduction of undesired side effects.

In this context, the most advanced nanomedical approaches for drug delivery are aimed to develop smart nanosized cages with specific cellular targeting (namely **active targeting**)<sup>11;16;17</sup>. Then, ligands that recognize specific molecules (biomarkers) overexpressed in the surface of the target cells can be anchored to the surface of the NPs (Figure 2). Note that specific accumulation in target cells is favored by multivalent display of ligands on nanoscale entities, which promotes multiple cell anchorage and enhanced nanoparticle wrapping.

The pursuit for the search and isolation of novel targeting moieties, including monoclonal antibodies and antibodies fragments (single-chain variable fragments and affibodies), small peptides or aptamers among others has become in recent years a priority goal<sup>18;19</sup>. Peptides present favorable characteristics over other ligands, including low molecular weight (around 1 kDa), ideal tissue penetration ability, low-cost of manufacturing and relative flexibility in chemical conjugation processes<sup>20;21</sup>. There are several methodologies for the screening of potential ligands among which phage-displayed library technology has emerged as a powerful tool for the identification and generation of peptides and antibodies<sup>20</sup>.

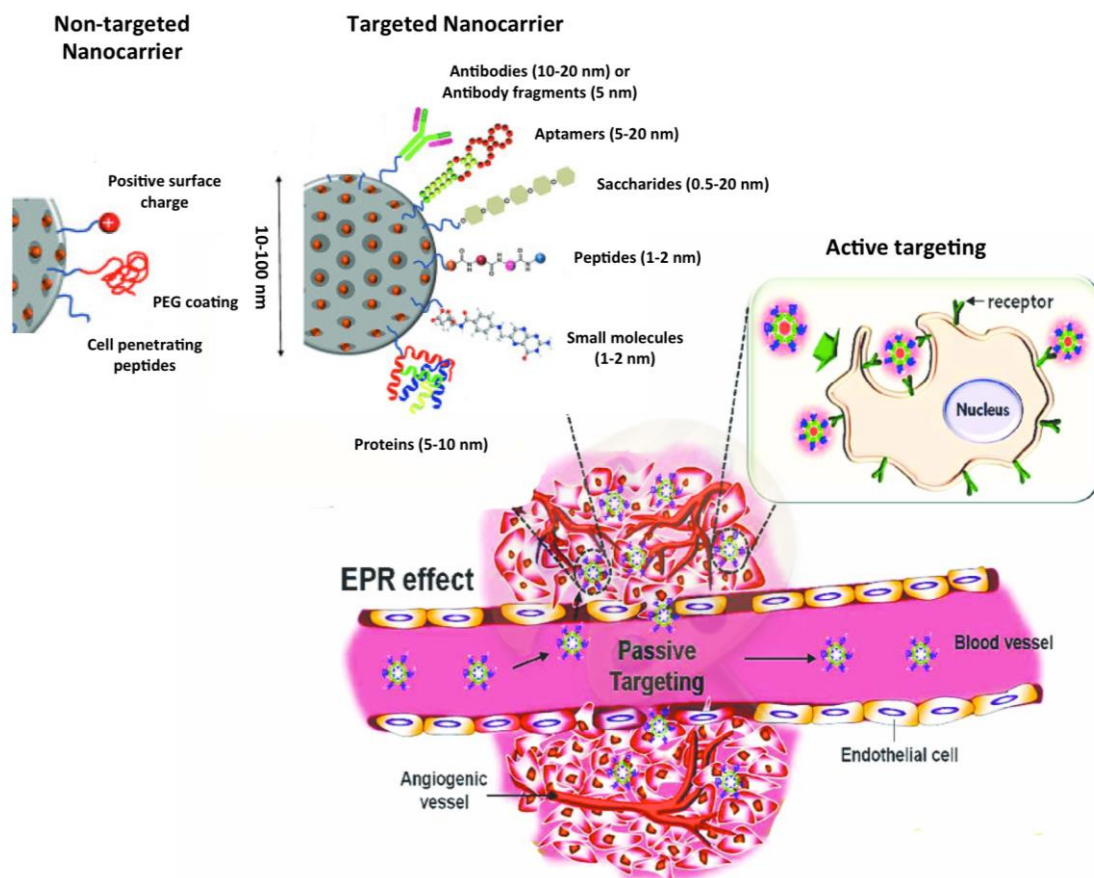


**Figure 2:** Passive/active tissue targeting. Nanoparticles reach the targeted tissue through EPR effect. Nanoparticles with specific surface ligands can specifically internalize into the target cell and release the cargo in the required subcellular compartment. Modified from<sup>22</sup>.

## 1.2. PHYSICOCHEMICAL PROPERTIES OF NANOPARTICLES.

The exploration of nanoparticle's physicochemical properties is a fundamental requirement for the material reproducibility and pharmaceutical regulators approval as they will determine nanoparticle recirculation and correct transit from the administration point to the target cell (Figure 3)<sup>7</sup>.

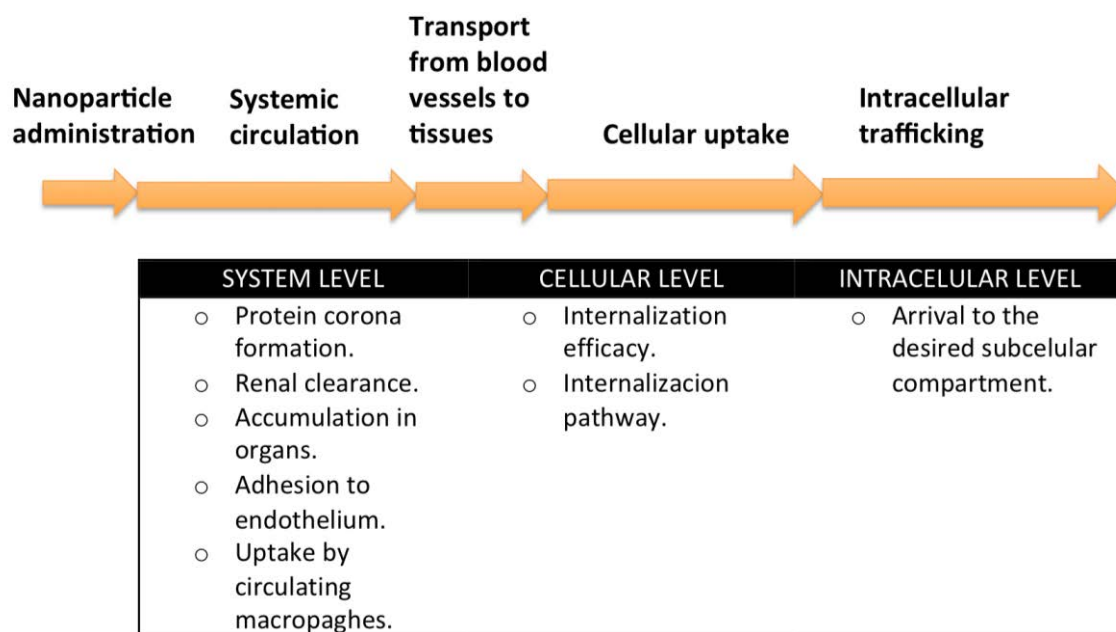


**Figure 3:** Different biological barriers and processes that NPs have to overcome or fulfill respectively for a proper biodistribution after their systemic administration in the body.

### 1.2.1. SYSTEM LEVEL.

**SURFACE:** Immediately after the NPs come in contact with plasma, proteins are adsorbed to the particle surface, namely **protein corona**, a phenomena that occurs mainly with positively charged and hydrophobic NPs<sup>23;24</sup>. In this process of protein adsorption, immunoglobins and complement proteins are the predominant contributors leading to the opsonization of the NPs and thus, their removal by the cells of the reticuloendothelial system (RES). This process along with the triggering of hypersensitivity reactions due to the complement activation, complicates targeted drug delivery.

NPs with neutral and negative surface charges reduce the protein corona having longer circulation half-lives and lower accumulation in liver and spleen whereas positively charged NPs usually show higher opsonization and toxicity such as haemolysis and platelet aggregation<sup>25</sup>.

Current methods for addressing opsonization process have focused on rendering the particle surface more hydrophilic or by neutralizing the particle's surface charge. Nowadays, the predominant strategy is based on the addition of hydrophilic polymeric



coating, such as polyethylene glycol (PEG), to the surface of the particle<sup>26</sup>. PEG increases drug hydrophilicity, impairs uptake by reticuloendothelial cells, minimizes clearance by neutralizing antibodies, and reduces renal filtration. Even if the therapeutic effect is enhanced, PEGylation could inhibit cellular uptake and subsequent endosomal escape<sup>27;28</sup> and also, PEG effect could be transient, so eventual opsonization and macrophage clearance still occurs<sup>29</sup>.

**SIZE:** For intravenously injected engineered NPs, size is one of the most important parameters affecting biodistribution. Particles smaller than 6 nm are rapidly cleared from the circulation through **renal clearance**<sup>25;30;31</sup>, and as particle size increases from 100 nm on, **accumulation in different organs** such as the liver, the spleen and lungs can occur<sup>7</sup>. Specifically, large NPs are filtered by sinusoids in the spleen (vascular fenestrations are typically between 200-500 nm), by noncontinuous endothelia in the liver (vascular fenestrations measure 100 nm) and they can be also accumulated within capillaries of the lungs (from 200 nm for intravenously injected NPs and in the micrometer range for inhaled particles). Accumulated NPs in organs are usually uptaken and removed by the RES. Thus, size between 10 and 100 nm seems to be the optimal one to achieve longer circulation time.

Moreover, larger NPs, having bigger surface, show major **protein corona** and higher opsonization process being more easily recognized by the complement system<sup>32-34</sup>.

**SHAPE:** The circulation half-life of a particle is also affected by shape. For instance, discoidal particles show unique dynamics that favor **adhesion to endothelium** compared to spherical particles that tend to align with blood flow<sup>35-37</sup>.

On the other hand, geometrical parameters as curvature and particle size ratio, affect to the **uptake by circulating macrophages**<sup>38;39</sup>. Indeed, having a low ratio and maximal curvature, spherical particles are more easily uptaken than ellipsoidal, cylindrical and discoidal particles that show longer circulation life times.

**DEFORMABILITY:** Different studies suggest that NPs prone to deform have reduced **accumulation in organs** such as the spleen and liver compared with rigid NPs<sup>40</sup>.

### 1.2.2. CELLULAR LEVEL.

**SURFACE:** One important issue of passive targeting is that it does not induce cell internalization once within the target tissue, so ligands should be incorporated into surface design to induce accumulation into target cells. Depending on the anchored moieties in the surface of the NPs, **internalization pathway** is altered. Generally, cell penetrating peptides (CPPs) facilitate non-specific cell entrance<sup>41</sup> whereas ligands that recognize specific surface receptors promote the endosomal uptake of the nanomaterials<sup>16;17</sup>.

On the other hand, the **cell internalization efficacy** is also altered by surface charge. In general, due to the cell membrane's negative surface, positively charged particles trigger more non-specific internalization<sup>42</sup>.

**SIZE:** Avidity (the strength with which a non-covalent attachment to a target molecule occurs) and multivalency (multiple ligands superficially exposed) are key parameters in the **cell internalization efficacy** of the NPs and is directly dependent on NP size<sup>43;44</sup>. Both, avidity and multivalency are increased by a large surface/volume ratio. Thus, very small NPs show poor number of ligands exposed in the surface and reduced avidity (or in other words, elevated ligand/receptor dissociation constant). In this context, very small NPs show low ligand density and poor avidity and may not remain enough time attached to the membrane to internalize properly whereas very big NPs can strongly attach saturating available receptors and limiting cell internalization. Therefore, the optimal NP size to proper receptor mediated internalization has been described to be between 25 and 50 nm<sup>43-45</sup>.

On the other hand, size is also related to **internalization pathway**<sup>45;46</sup>. Some studies revealed that 15 nm NPs show a higher endocytotic rate than 100 nm NPs although in other studies, 50 nm NPs display the maximum cellular uptake. Moreover, NPs smaller than 200 nm tend to internalize via clathrin mediated endocytosis and the ones that are between 200-500 nm internalize through caveolae mediated endocytosis. Important volumes of data have been collected about size-dependent internalization but the relation remains unclear and contradictory results have been obtained, probably because cell uptake depends on multifactorial factors such shape,

nanomaterial and cell type.

**SHAPE:** Spherical NPs show higher **cell internalization efficacy** since the membrane bending energy is minimal compared to rods, cylinders or disc-shaped NPs<sup>47;48</sup>. However, when considering NPs larger than 100 nm, rods or discoidal particles display higher surface area and thus more multivalent interactions that provide them with better internalization rates<sup>49</sup>.

**1.2.3. INTRACELLULAR LEVEL.**

**SIZE:** The delivery of the drug to the desired subcellular compartment could be affected by NP size. Indeed, when **reaching cell nucleus** is necessary for the therapeutic action, NPs bigger than 10-30 nm (40kDa) will not be able to go inside by passive diffusion since nuclear pore complex size is around 55 Amstrong<sup>50;51</sup>. This can be solved by using nuclear localization signals that display the active transport mechanism.

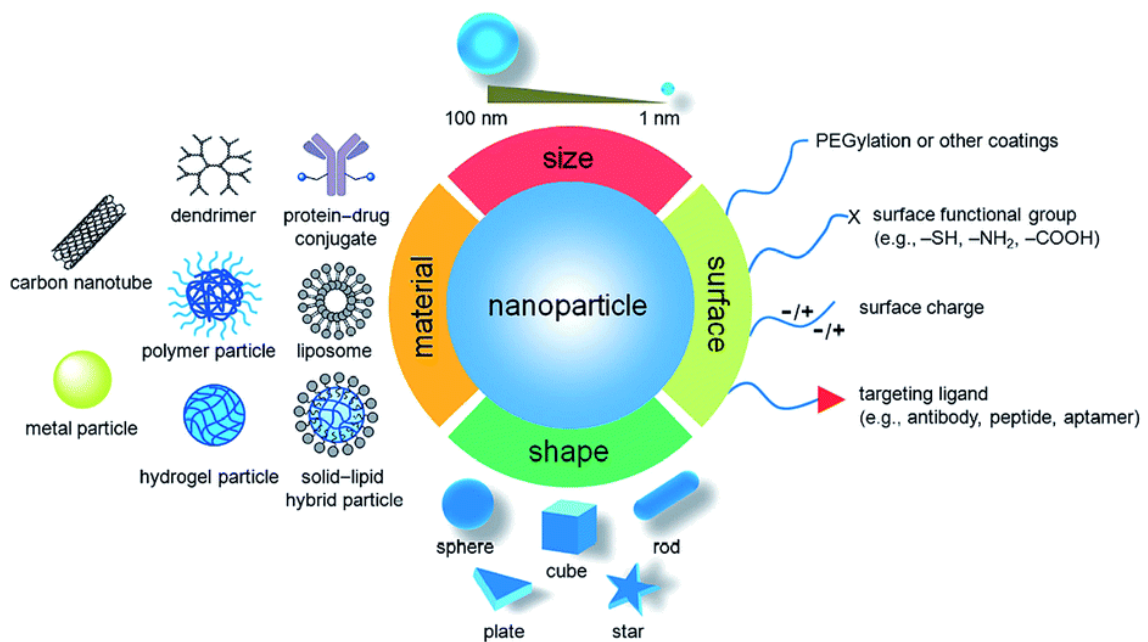


**Figure 4:** A summary of bio-physicochemical properties and materials of NPs that have been explored as carriers for drug delivery<sup>52</sup>.

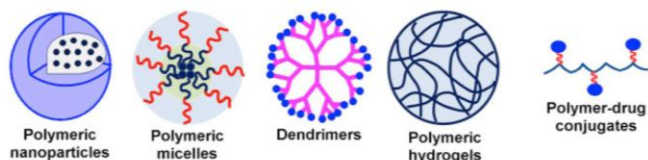
### 1.3. BIOCOMPATIBILITY.

Many materials have been so far explored for the production of nanocontainers. Several types of NPs are currently used for drug delivery<sup>53-55</sup> such as lipid-based NPs, polymer-based NPs, metallic NPs, carbon nanomaterials and protein-based NPs (Figure 5).

These materials, once nanostructured, show very interesting applications in medicine, electronics and environmental sciences. However, as drug delivery systems, most of these materials raise severe biocompatibility concerns such as poor water solubility and high immunotoxicity<sup>56;57</sup>. Indeed, certain NPs may induce allergic sensitization, can modulate cytokine production and have pro-inflammatory effects. Moreover, they are poorly degraded by human enzymes and tend to accumulate in lysosomes leading to lysosomal diseases.

In this regard, these issues can be possibly solved using **biodegradable materials** as natural polymers or proteins.

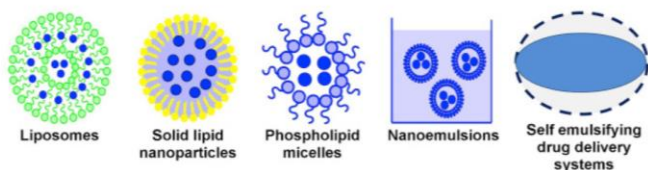
#### POLYMERIC NANOCARRIERS



**Advantages:** Well characterized, biocompatibility and versatility in terms of chemical composition.

**Disadvantages:** Poor degradation of the carrier, rapid clearance by RES.

#### LIPID-BASED NANOCARRIERS



**Advantages:** Effectively delivers water-soluble and insoluble drugs, biocompatibility.

**Disadvantages:** Toxicity, rapid clearance by RES, low drug loading capacity, low solubility.

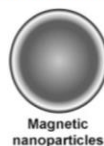
#### METAL NANOCARRIERS



**Advantages:** Quantum dots: fluorescent properties for imaging and drug tracking. Gold/silver NPs: thermoablative therapies, photodynamic therapies.

**Disadvantages:** Non-biodegradability, limited biocompatibility, high cost for large scale production.

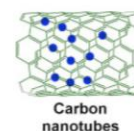
#### MAGNETIC NANOCARRIERS



**Advantages:** Influenced by exterior magnetic field for imaging and drug delivery.

**Disadvantages:** Non-biodegradability, limited biocompatibility, poor colloidal stability.

#### CARBON-BASED NANOCARRIERS



**Advantages:** Near infrared emissions allow for tissue imaging and diagnosis.

**Disadvantages:** Non-biodegradability, toxicity by oxidative stress.

Figure 5: Different kinds of nanocarriers used for drug delivery.

## 2. APPLICATIONS OF THERAPEUTIC NANOPARTICLES.

In the past two decades, several nanoparticle-based therapeutics have been successfully introduced for the treatment of many diseases<sup>58</sup>. Oncology, Central Nervous System (CNS) indications and Infections represent major focuses of the nanopharmaceutical research effort (Figure 6)<sup>59</sup>.

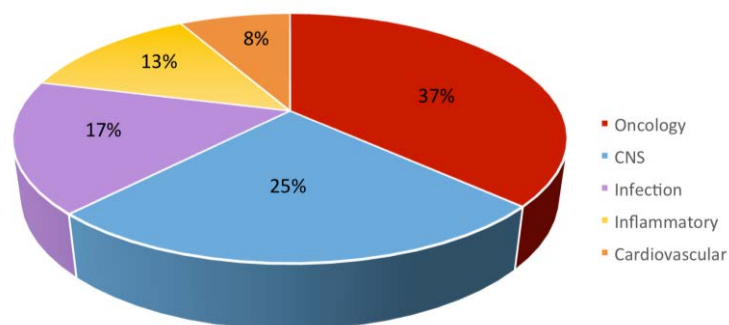


*Figure 6:* Nanopharmaceutical global market share by therapeutic indications<sup>59</sup>.

### 2.1. ONCOLOGY.

Cancer remains one of the leading causes of death in most parts of the world<sup>60</sup>. After surgical removal, chemotherapeutics are regularly and systemically administered to patients as main therapy but unfortunately, therapeutic effect remains insufficient. Chemotherapeutics, having small molecular size (below renal filtration cut-off, namely 6-8 nm) and lacking specificity, show short circulation time, limited accessibility to the tumor tissue and metastatic sites, and intolerable toxicity that leads to the damage of active and fast growing healthy cells such as bone marrow, gastrointestinal or liver cells, strongly limiting administrable therapeutic dose<sup>61</sup>.

Development of multi-drug resistance and the dynamic heterogeneous biology of the growing tumors are also related with their poor efficacy<sup>62;63</sup>. The use of targeted NPs as vehicles for these drugs significantly increases efficiency of the delivery into the cancer cells, reduce drug dosage and mitigates side effects<sup>64</sup>.

### **2.1.1. TARGETING STRATEGIES.**

Most of the approved nanomedicines for oncology rely on **passive targeting** and therefore, EPR effect<sup>13;65</sup>. Unlike the tight endothelium of normal blood vessels, the vascular endothelium in tumor microvessels is discontinuous and leaky. The higher size of gaps between the endothelial cells (ranging from 100-780 nm), the high vasodilation due to the elevated levels of growth factors like VEGF (vascular endothelial growth factor) and bFGF (basic fibroblast growth factor) and the impaired lymphatic drainage in tumor tissues result in an enhanced accumulation of drugs in tumor tissues. Moreover, cell penetrating peptides (CPPs) such as the trans-activating transcriptional activator (Tat) peptide, have been used to promote non-specific cell internalization of accumulated NPs<sup>66</sup>. In 1994, PEG–L-asparaginase (Oncospar; Enzon) became the first nanostructured therapeutic to receive Food and Drug Administration (FDA) approval, for the treatment of acute lymphocytic leukaemia. The first liposome-based therapeutic, liposome-encapsulated doxorubicin (Doxil; OrthoBiotech), was approved by the FDA in 1995 for the treatment of HIV-related Kaposi's sarcoma and the treatment of ovarian cancer and multiple myeloma. However, passive targeting suffers from serious limitations<sup>67</sup> such as inefficient drug diffusion into tumor cells<sup>68</sup>, the random nature of targeting and the fact that the EPR effect is a highly heterogeneous phenomenon, which varies substantially from tumor model to tumor model, as well as from patient to patient<sup>69;70</sup>.

Regarding to the **active targeting** approach, cancer cells express some new molecules and/or over-express specific own molecules in comparison to normal cells due to their transformed nature, ranging from mutant genes and RNAs, to proteins, lipids and even small metabolite molecules. These molecules can serve as significant biomarkers for the progression of disease and also as tumoral markers for drug delivery. For example, many types of cancer cells over-express transferrin and folate receptors because of the high metabolic demands and rapid proliferation; thus, conjugation of transferrin<sup>71-73</sup>, folic acid<sup>74-76</sup> or specific antibodies<sup>77;78</sup> have been a common targeting approach used for engineered NPs. However, these receptors are also expressed to some degree on non-target cells leading to significant toxic off-target effects<sup>79</sup>. Recently, selective

targeting strategies rely on highly specific interactions of de novo designed antibodies, aptamers, peptides and oligonucleotides with tumor cell surface receptors.

Moreover, note that NPs, once they have bound to the receptor, are internalized through endocytic pathway and destined to a lysosomal compartment. Therefore, before the fusion with a lysosome, endosomal escape must occur to prevent degradation of the cargo under harsh lysosomal conditions and to allow access of the carrier to the desired subcellular compartment, whether it is the cytosol, the mitochondria or the nucleus. This can be accomplished through proton sponge effect by using cationic surface groups such as His-rich peptides<sup>80;81</sup> and polyethylenimine (PEI)<sup>82;83</sup> or by adding peptides able to disrupt endosomal membrane like influenza virus hemagglutinin peptide (HA2)<sup>84;85</sup> or antimicrobial peptides as natural Mellitin or synthetic GWH1<sup>86;87</sup>.

### COLORECTAL CANCER TARGETING.

Colorectal cancer (CRC) is the third most common cancer as well as the third cause of mortality worldwide. First-line chemotherapeutic treatment of CRC comprises intravenous 5-Fluorouracil (5-FU) administration in combination with oxaliplatin, increasing the response of the therapy up to 50 % compared with 15 % for 5-FU monotherapy<sup>88</sup>. Unfortunately, traditional therapy induces tumor cell death and shrinkage but is suggested to grow back due to selective resistance of a subset of cells that have cancer stem cell potential<sup>89;90</sup>.

**Cancer stem cells** (CSCs) are the tumorigenic root of cancers due to their clonogenic and high self-renewal capacity. Recent studies have highlighted the principal role of CSCs in tumor recurrence, relapse and metastatic dissemination<sup>91</sup>. Colorectal CSCs are among the most difficult to kill and the development of hepatic metastases is the main reason of mortality in colon cancer patients<sup>92</sup>.

Recent identification of surface markers over-expressed in colon CSCs such as CD133, CD166, CD44, CD24, CXCR4, beta1 integrin-CD29, Lgr5, EpCAM (ESA), ALDH-1, Msi-1, DCAMLK1 or EphB receptors, allows the development of treatment strategies that can specifically eliminate colon CSCs and enable a long-lasting clinical response that



controls metastatic process<sup>90;93</sup>.

Among them, cytokine receptor CXC chemokine receptor type 4 (**CXCR4**) plays a critical role in determining the metastatic destination to the liver, bone marrow and lungs where its ligand SDF-1 is abundant<sup>94-96</sup>. Indeed, patients with high CXCR4-expressing tumors have increased risk of local recurrence and distant metastases<sup>97;98</sup>, and also CXCR4 expression is higher in the metastases compared to primary tumors<sup>99;100</sup>. This offers preclinical evidence that blockade of the SDF-1/CXCR4 and depletion of CXCR4<sup>+</sup> cell population is a promising therapeutic strategy to achieve metastatic control in colon cancer<sup>101-104</sup>.

### **2.1.2. NANOMATERIALS AND BIOCOMPATIBILITY.**

Most of the approved and clinically used nanomaterials for oncology are still based in lipids and polymers (Table 1)<sup>59;105</sup>.

**Liposomes** are a lipid bilayers composed of amphipathic phospholipids (mainly phosphatidyl cholines) that enclose an interior aqueous space. These carriers not only target drug upon functionalization with cell specific ligands and protect them from degradation, but they can also be made temperature or pH sensitive, conferring the ability to release the drug in the specific site of action<sup>106</sup>. However, their use as DDS has been restricted due to inherent health issues such as low encapsulation and storage efficiency, poor stability and also, difficulties concerning scaling-up for clinical evaluation<sup>107</sup>.

**Polymeric NPs** promise some interesting advantages over liposomes. For instance, this NPs allow chemical conjugation of the drug to their surface and increase the ratability of drugs<sup>106</sup>. However, they can also evoke side effects; anaphylaxis or platelet dysfunction have been reported for dextran (glucose polymers)<sup>108;109</sup> and serious toxicity problems have been described for dendrimers (repeatedly branched, roughly large spherical large structures)<sup>110</sup>. The copolymer poly(lactic-co-glycolic acid) (PLGA) is the most common natural biodegradable polymer approved as a compatible biomaterial used to overcome side-effects imposed by other polymers<sup>111;112</sup>, however, PLGA NPs show 40 % particle accumulation in liver, limiting its use in clinics<sup>113</sup>.

**Table 1:** Principal nanoparticle-based drug delivery systems in clinical trials for oncology<sup>59</sup>.

<b>Delivery system</b>	<b>Name</b>	<b>Administ.</b>	<b>Active molecule</b>	<b>Indication</b>	<b>Status</b>
<b>Protein-based delivery systems</b>					
Nab-technology	ABI-009	I.V.	Rapamycin	Non-muscle invasive bladder cancer	Phase I/II
<b>Polymer-based delivery systems</b>					
Transdrug PACA NPs	Livatag	I.V.	Doxorubicin	Hepatocellular carcinoma	Phase III
Cyclodextrin-based NPs	CRLX101	I.V.	Camptothecin	NSCLC	Phase II completed
PSMA-targeted PEG-PLA/PLGA NPs	BIND-014	I.V.	Docetaxel	NSCLC	Phase II completed
PEG-PLA/PLA NPs	–	I.V.	Docetaxel	Solid tumors	Phase I
PEG polyamino acid NPs	NC-6004	I.V.	Cisplatin	Solid tumors	Phase I/II
Core cross-linked polymeric micelles	CriPec	I.V.	Docetaxel	Solid tumors	Phase I
<b>Lipid-based delivery systems</b>					
Lipid NPs	Atu-027	I.V.	PKN3 siRNA	Pancreatic cancer	Phase IIb
Lipid NPs	DCR-MYC	I.V.	MYC siRNA	Hepatocellular carcinoma	Phase I/II
Lipid NPs	TKM-080301	I.V.	PLK1 siRNA	Liver cancers	Phase I completed
Liposomes	NDL02-s0201	I.V.	HSP47 siRNA	Hepatic fibrosis	Phase Ib/II
Liposomes	–	I.V.	P53 DNA plasmid	Glioblastoma	Phase II
Anti-EGFR liposomes	–	I.V.	Doxorubicin	Solid tumors	Phase I completed

## 2.2. INFECTIOUS DISEASES.

Infectious diseases are caused by the presence and growth of pathogenic biological agents like bacteria, fungi, parasites etc. in the host organism and it is characterized by the presence of clinical symptoms. Nanoparticle-based drug delivery platforms including liposomes, polymeric NPs, dendrimers, and various inorganic NPs have been increasingly exploited to deliver and enhance the therapeutic effectiveness of existing antibiotics<sup>114</sup>.

However, the treatment of bacterial infection still faces significant challenges, particularly the emergence of antibiotic resistance<sup>115;116</sup>. In this context, naturally occurring cationic antimicrobial peptides (AMPs) are of special interest because of their potential as alternatives to conventional antibiotics<sup>117</sup>.

### **2.2.1. TARGETING STRATEGIES.**

**Passive targeting** and the enhanced permeation and retention (EPR) effect can be exploited by NPs for antibiotic/AMPs delivery<sup>118</sup>. At infection sites, the release and accumulation of bacterial components (mainly bacterial proteases and lipopolysaccharide or lipoteichoic acid) trigger various inflammatory mediators that directly stimulate vascular permeability<sup>119;120</sup> and also activate immune cells that interact with vascular endothelia<sup>121</sup>. This leads to gap widening and barrier dysfunction, increasing permeability and favouring nanoparticle accumulation at the sites of infection. As an example, PEGylated liposomes have been shown to accumulate by passive targeting at soft tissue infected by *Staphylococcus aureus*<sup>122;123</sup>.

**Active targeting** has shown to be also a good approach against infectious diseases<sup>124</sup>. Vancomycin<sup>125;126</sup> that binds preferentially to gram positive bacteria, mannose-specific or fucose-specific lectins<sup>127;128</sup> that show enhanced binding affinity to the carbohydrate receptors on some bacteria surfaces, single-domain antibodies<sup>129</sup> and bacteriophage tail spike proteins<sup>130</sup>, among others, have been conjugated to NPs resulting in effective targeted delivery platforms against a variety of bacterial infections. Furthermore, aptamers have also become attractive targeting moieties extensively explored to target NPs to pathogenic bacteria such as *Salmonella typhimurium* and *Mycobacterium*

*tuberculosis*<sup>131;132</sup>.

In addition to ligands that recognize specific biomolecules, cationic peptides are highly interesting for effective bacterial targeting<sup>133-135</sup>. Note that pathogenic bacteria maintain a negative surface charge under physiological conditions. Therefore, cationic peptides are capable of binding bacterial cells via electrostatic interactions.

For example, a self-assembled cationic peptide nanoparticle has shown strong antimicrobial properties while inducing minimal systemic toxicity<sup>136</sup>. By using *Staphylococcus aureus*-infected meningitis rabbits it was demonstrated that these cationic NPs can cross the blood–brain barrier and suppress bacterial growth in infected brains. This strategy is attractive for its multivalent effect and the ability to target polymicrobial infections.

### **2.2.2. NANOMATERIALS AND BIOCOMPATIBILITY.**

**Metals** as silver, gold, zinc and graphene based NPs, have been the most used nanomaterials in infectious diseases. Indeed, some of them, due to their specific physicochemical properties, show intrinsic broad-spectrum antibacterial properties against both Gram-positive and Gram-negative bacteria. Then, they are very interesting for antimicrobial applications such as in antibacterial coatings for implantable devices and medicinal materials to prevent infection and promote wound healing, in bacterial detection systems to generate microbial diagnostics, in antibacterial vaccines to control bacterial infections and in antibiotic delivery systems to treat diseases<sup>124</sup>. According to existing research, the antibacterial effects of these NPs are<sup>137</sup>: 1) disruption of the bacterial cell membrane; 2) generation of reactive oxygen species (ROS) 3) penetration of bacterial cell membrane; and 4) induction of intracellular antibacterial effects, including interactions with DNA and proteins. For instance, silver NPs are being commercialized for antimicrobial activity<sup>138</sup>. Certain studies have proposed that Ag NPs are able to attach to sulphur containing proteins in bacterial cell membrane and prompt neutralization of the surface electric charge of the bacterial surface changing its penetrability and finally, leading to bacterial death<sup>139;140</sup>. Even though they show great effectiveness, silver NPs can cause blood-brain barrier (BBB) and liver destruction by producing ROS, as well as neuronal

degeneration and brain edema after intravenous administration<sup>141-143</sup>. Therefore, even their use in nanomedicine for treating wounds, burns and catheter related infections remains very interesting, their exploitation as drug delivery system in humans should be limited.

In this context, biocompatible nanocarriers that safely administer drugs have been taken to clinics in the last years, being **mainly liposome and polymeric based nanomaterials** (Table 2)<sup>59</sup>. Most important among the liposomal antimicrobial agents is FDA accepted Liposomal amphotericin B (AmBisome; Gilead Sciences, USA) that is used in aspergillosis, candidiasis, and cryptococosis. It has been also used as a therapy for human visceral leishmaniasis<sup>144</sup>. However, these lipid and polymeric based particles have limitations like absence of targeting, water solubility and toxic effects due to their poor biodegradability<sup>111;145</sup>.

**Table 2:** Main nanoparticle-based DDS in clinical trials for infectious diseases<sup>59</sup>.

Delivery system	Name	Administ.	Active molecule	Indication	Status
<b>Protein-based delivery systems</b>					
F Protein NPs	RSV-F vaccine	I.V.	RSV	RSV infections	Phase III
<b>Polymer-based delivery systems</b>					
PEI NPs	–	Local	No drug	Bacterial infections in HNC patients	Phase I
Alkylated PEI NPs	–	Local	No drug	Bacterial infections	Phase II
<b>Lipid-based delivery systems</b>					
Lipid crystal NPs	CAMB	Oral	Amphotericin B	Candidiasis	Phase II

## **2.3. CENTRAL NERVOUS SYSTEM DISEASES.**

### **2.3.1. TARGETING STRATEGY.**

The BBB is one of the most essential protection mechanisms in the CNS since it protects the brain from foreign substances in the blood that may damage the brain.

From the anatomic point of view, the BBB is mainly composed of pericytes, astrocytes, neurons, endothelial cells and junctional complexes<sup>146</sup>. Due to the presence of tight junctions instead of large fenestrations between endothelial cells, as well as high electrical resistance (1500-2000  $\Omega$  cm<sup>2</sup>) between the endothelial cells caused by the encapsulation of capillaries by pericytes and astrocytes, the passage of the drugs through the BBB is primarily restricted. Indeed, only small molecules in the order of 400-500 Da such as water, some gases, and some lipid-soluble compounds can easily penetrate through the BBB by passive transcellular diffusion.

Although the delivery of drugs into the brain is a challenging field, it attracts much attention due to the increasing population of neurodegenerative diseases such as Alzheimer's, Parkinson's and Huntington's disease, and encephalitis associated to HIV infection.

Different approaches to transport large molecules with high electric charge, polarity and hydrophilicity (i.e., glucose, amino acids and most drugs) across BBB have been explored<sup>147-149</sup> (Figure 7).

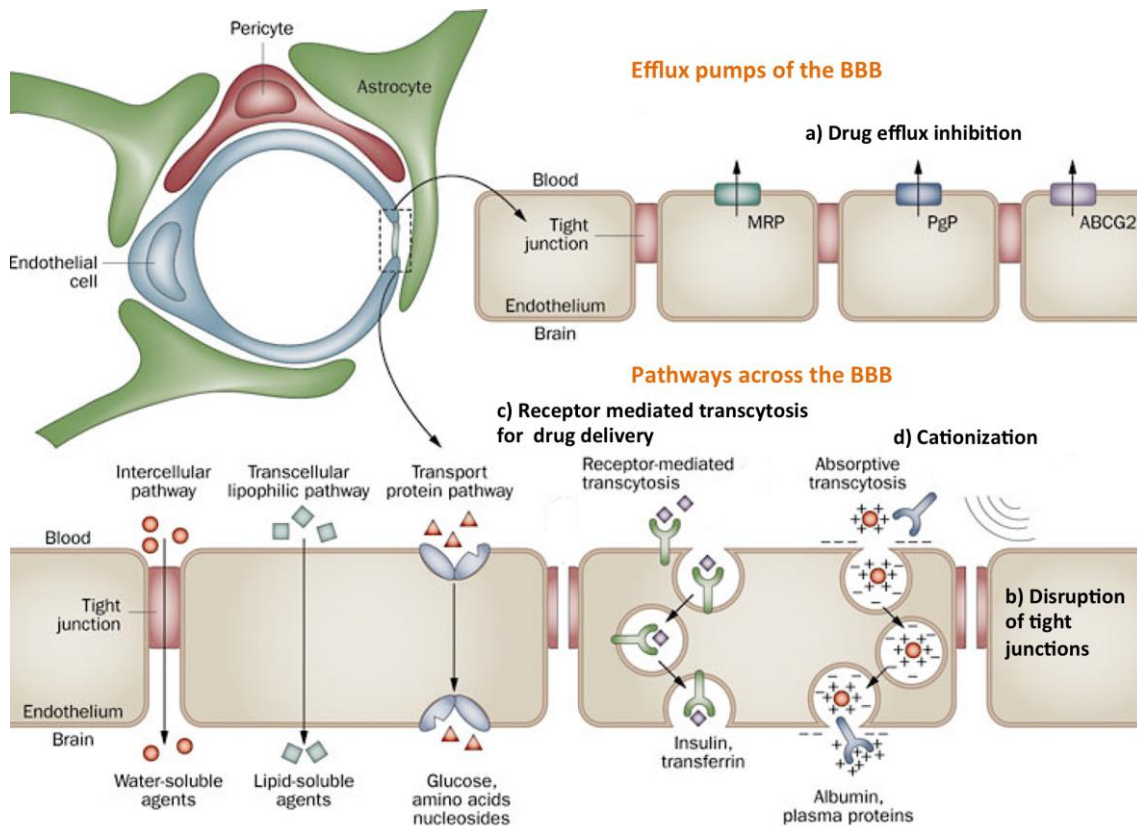


**Figure 7:** Approaches to enhance drug delivery to the brain. a) The main drug efflux transporters of brain capillary endothelial cells include MRPs, PgP, and ABCG2. All of these transport proteins have been targeted for pharmacological inhibition such as probenecid for MRPs, verapamil for PgP and GF120918, for ABCG2. b) Tight junctions normally restrict penetration of water-soluble compounds across the BBB, but they can be disrupted by mechanical and pharmacological methods, via ultrasound and bradykinin analogs, respectively. c) Receptor-mediated transcytosis has been used to increase transport of drugs across the BBB, and d) cationization can increase uptake of molecules by absorptive transcytosis. Abbreviations: ABCG2, breast cancer resistant protein; BBB, blood–brain barrier; MRPs, multidrug resistant proteins; PgP, P-glycoprotein. Adapted from <sup>150</sup>.

NP-mediated drug delivery is emerging as an effective and non-invasive system to assist drugs to cross the BBB through **receptor mediated transcytosis**<sup>148;151</sup>. It has been reported that different receptors are highly expressed on the endothelial brain cells such as low density lipoprotein (LDL), transferrin and insulin receptors<sup>152;153</sup>. Therefore, the functionalization of NPs with peptides that recognize these receptors and induce transcytosis has been deeply explored to deliver drugs through the BBB.

De novo peptides that efficiently bind to these receptors can be identified by different techniques. As an example, Angiopep was obtained by kunitz domain libraries and is



derived from aprotinin. This peptide exhibits high LDLR binding efficiency and has been used for glioma-targeting delivery by several research groups<sup>154-157</sup>. Seq1 is a novel peptide ligand obtained by phage display technique, able to target and transmigrate across the BBB<sup>158;159</sup>. Thus, the use of these peptides to enable NPs to penetrate through the BBB is an attractive approach.

### **2.3.2. NANOMATERIALS AND BIOCOMPATIBILITY.**

NPs that carry drugs into the brain include a variety of nanomaterials<sup>160;161</sup> such as lipid based NPs, polymer based NPs, nanoemulsions, dendrimers, metal NPs...

**Lipid NPs**, such as cationic liposomes, solid lipid NPs and nanostructured lipid carriers, have been extensively studied for drug delivery to the brain. One application is the PEGylated liposomes, encapsulated with FK506 (Tacrolimus), that were used to treat cerebral ischemia reperfusion injury<sup>162</sup>.

**Polymeric NPs** are another extensively used DDS targeting CNS. For instance, polybutyrcyanocrylate coated with ApoB and ApoE showed promising permeability and dendrimers formed by poly(amidoamine) were synthesized with transferrin on the surface to enhance BBB transport<sup>163;164</sup>. One of the latest studies described the effect of modifying the surface of polymeric NPs on drug delivery across BBB.

**Nanoemulsions** are another novel DDS formed by oil and water emulsions<sup>165</sup>. The average size of the nanoemulsion ranges from 100 to 500 nm. Saquinavir mesylate (SQVM) is a poorly BBB permeable anti-HIV drug. By incorporating SQVM into the nanoemulsion nanoparticle, the bioavailability increases drug permeation rate significantly<sup>166</sup>.

However, as we have mentioned before, all these nanocarriers present some issues that limit their use in clinics.

### 3. PROTEIN-BASED NANOPARTICLES.

The poor biodegradability and toxicological effects showed by the currently and most used nanomaterials for the generation of NPs have imposed the introduction of novel biocompatible and biodegradable materials, as natural polymers or proteins. The accumulation of some administrated biodegradable polymers such as PLGA in some organs is also a matter of concern. In this context, protein-based nanomaterials appear to be the most appealing ones for drug delivery due to their high biocompatibility and biodegradability, their natural structural roles, their simple and cost effective biological production and their functional versatility by genetic engineering (Figure 8)<sup>167;168</sup>.

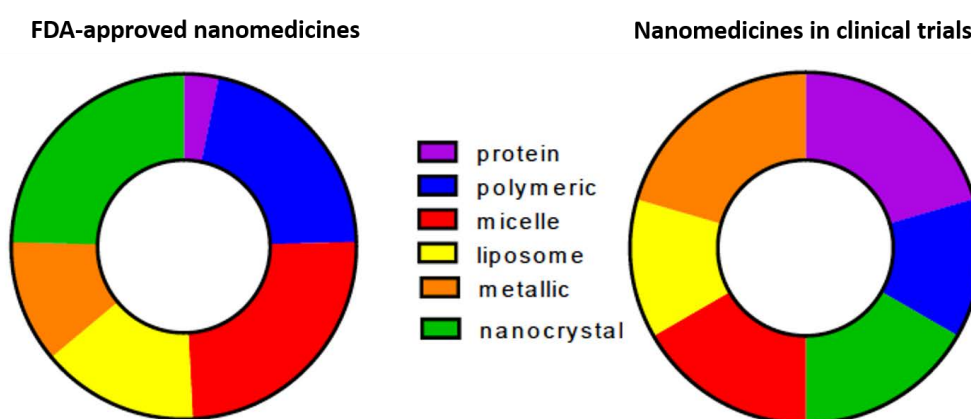


**Figure 8:** FDA-approved nanomedicines from 2001-2015 and nanomedicines under clinical trials cataloged by material. Modified from <sup>169</sup>.

#### 3.1. DRUG-LOADED PROTEIN NANOPARTICLES.

Synthetic protein NPs generated by different procedures, antibodies and protein assemblies are the most important protein-based nanocarriers developed for drug delivery (Figure 9).

Drugs are usually conjugated to the protein carrier by lysine-amine and cysteine-thiol coupling by amine-activated ester/carboxylic acid and thiol-maleimide chemistries, respectively<sup>170;171</sup>. Moreover, targeting agents can also be attached to the carrier by a chemical linker that has to maintain the proper biodistribution conferred by the targeting agent and importantly, must remain stable during the extracellular phases of the delivery process<sup>172</sup>.

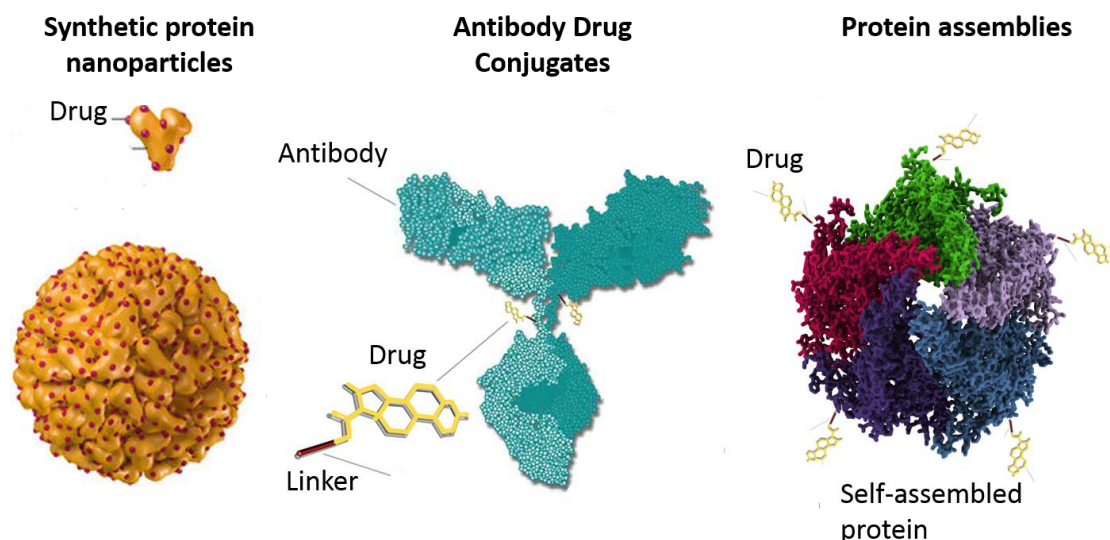


**Figure 9:** Schematic representation of different protein drug-loaded NPs.

### **3.1.1. SYNTHETIC PROTEIN NANOPARTICLES.**

Synthetic protein NPs have been successfully synthesized from various natural proteins including water-soluble proteins (e.g., bovine and human serum albumin) and insoluble proteins (e.g., zein and gliadin)<sup>173</sup>. During nanoparticle formation, the protein undergoes conformational changes that are usually based on unfolding of proteins that expose interactive groups such as disulfides and sulfhydryles and subsequent thermal or chemical crosslinking that result in NPs with entrapped drug molecules<sup>174</sup>. This process depends on its composition, concentration, crosslinking and preparation conditions such as pH, ionic strength, and type of solvent<sup>175</sup>. Coacervation/desolvation and emulsion-based methods are most commonly used for the preparation of these NPs<sup>173;176</sup>. Furthermore, targeting ability can be conferred through NP functionalization.

A paradigm of how proteins are incorporated as carriers of small molecular drugs in oncology is Abraxane, first FDA-approved for breast cancer in 2005. Abraxane is a nanostructured complex (sized 130 nm) formed by non-covalent hydrophobic interaction and high-pressure homogenization of human albumin and paclitaxel. This results in a nanoparticle colloidal suspension that is used in metastatic breast, pancreatic, and non-small lung cancers<sup>177</sup>.

### 3.1.2. ANTIBODY DRUG CONJUGATES.

Antibody drug conjugates (ADCs) are also representative complexes of protein drug-loaded carriers. They are based on a cytotoxic drug bound to a monoclonal antibody (mAb), Fv fragments or Fab fragments (Figure 10) directed against cell-surface markers. In this simple fusion strategy, the Ab or Ab derivatives confer the nanoscale size as well as specific targeting<sup>172;178</sup>. Microtubule inhibitors including maytansinoids (DM1/DM4) and auristatins (in form of monomethyl auristatin E/F: MMAE, MMAF) are the most commonly used drugs in ADCs. Unfortunately, ADCs only confer monovalent or divalent binding to the target cells and require highly potent payload drugs, due to their poor penetrability into the tumor tissue (only 1 % of the injected ADCs reach the tumor) leading to frequent life-threatening toxicities<sup>179</sup>.

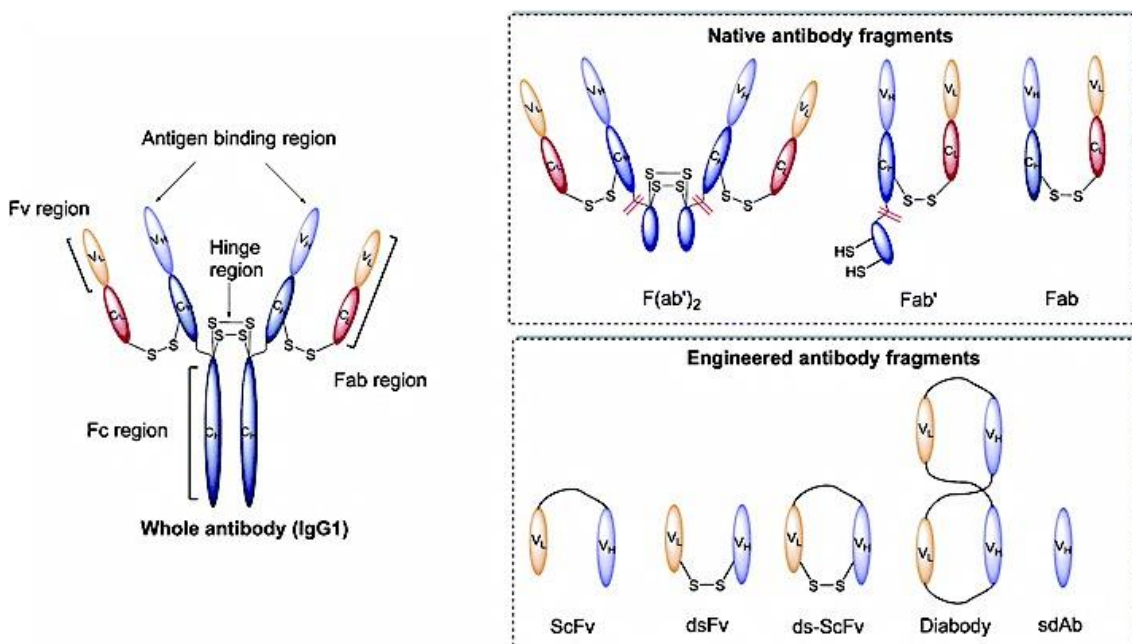


**Figure 10:** The basic structure of a conventional full size antibody and of common antibody fragments used for ADCs<sup>180</sup>.

### 3.1.3. PROTEIN ASSEMBLIES.

Protein assemblies have been also explored for nanomedical purposes and more especially for targeted drug and nucleic acid delivery (Figure 11)<sup>181;182</sup>. The notion of protein self-assembly into sophisticated architectures is prevalent in nature. All kind of protein structures are presented in a variety of organisms (e.g. viruses, bacteria, plants, mammalian cells), including cage-like architectures<sup>183;184</sup>. However, the poor functional flexibility, tunability and limited controlled-geometry from the natural occurring nanocages have encouraged research on de novo designed protein assemblies.

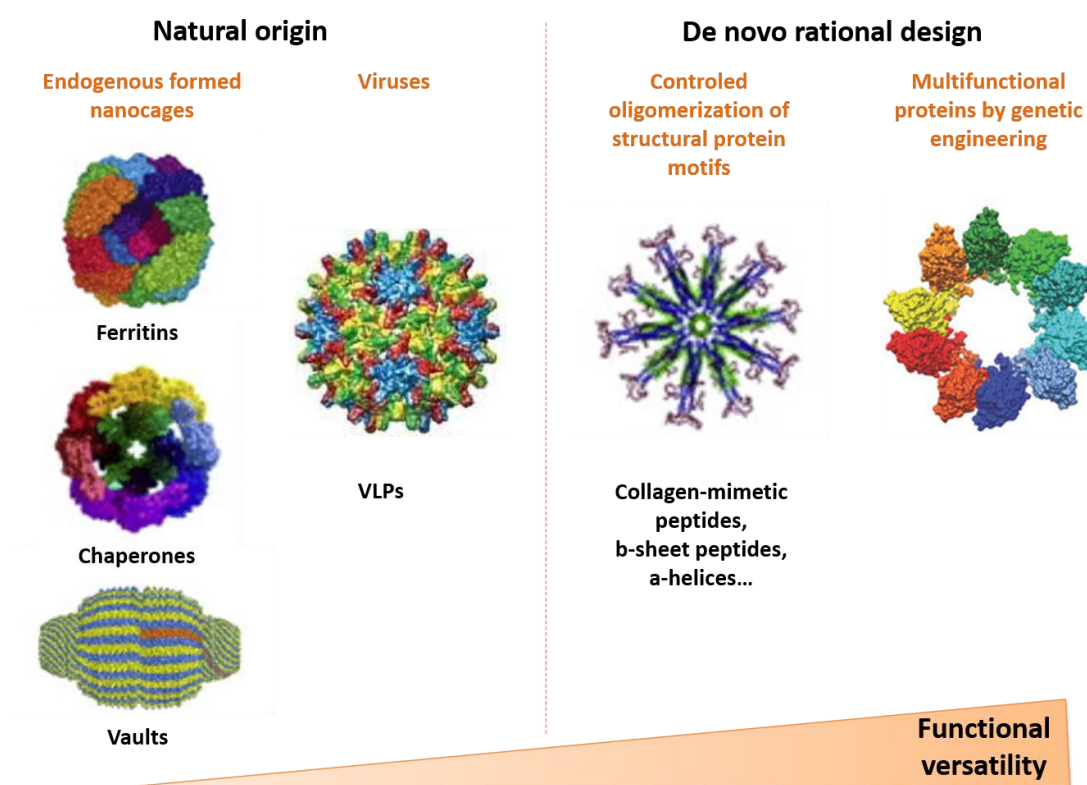


**Figure 11:** Schematic representation of different protein assemblies found in nature and de novo designed particles.

#### NATURAL ORIGIN.

Most of the **endogenous nanocages** are formed by self-assembly processes and include ferritins that are produced in almost all living organisms and regulate iron homeostasis<sup>185;186</sup>, small heat-shock proteins which are expressed in response to

cellular stress and promote proper folding of proteins<sup>187;188</sup> and finally, vaults that are highly conserved in eukaryotic cells and are involved in nuclear cytoplasmic transport, mRNA localization, nuclear pore assembly and also innate immunity<sup>189;190</sup>. These cage-like proteins provide spatial control to biological processes and also carry compartmentalized compounds that may be toxic or unstable for cell function.

Other well-studied examples in nature of self-assembling protein cages are **viruses**. Most viruses commonly consist of hundreds of protein subunits that self-assemble into a protein coat, which stores and protects viral DNA or RNA. Viruses, being strict intracellular parasites, are natural vectors for cell targeted nucleic acid delivery<sup>191</sup>. Structural proteins from some viral species can be recombinantly expressed and spontaneously assembled into virus-like particles (VLPs). VLPs are natural self-assembling constructs consisting of non-replicative viral capsids, lacking the viral genome. They have been used as protein vaccines<sup>192-194</sup> and they can also act as protein cages transporting therapeutic compounds to their natural target cells<sup>195-197</sup>. A variety of viral families have been engineered including retroviruses, lentiviruses, adenoviruses or adeno-associated viruses. All of them offer different properties regarding cell tropism, integration ability and quiescent cell infection capacity. Even though they are extremely efficient for gene therapy approaches, they show several restrictions, such as limited DNA-carrying capacity, high associated immune toxicity and biosafety aspects<sup>198</sup>.

### **DE NOVO RATIONAL DESIGN.**

The understanding of these natural protein nanocages and structure–function relationship of proteins may inspire the creation and engineering of novel protein cages to create smart, powerful nanocarriers for drug delivery.

Among the different assemblies that have been produced de novo, DNA origami represents the foremost example of this approach<sup>199</sup>. Short synthetic oligonucleotides are employed to fold the DNA genome of M13 phage into definable and computationally predictable structures. Indeed, the main advantage of DNA assemblies is that they are based on the Watson-Crick nucleic base complementarity, so there are only two different base pairs based on a specific pairwise interaction providing a reliable prediction of the structure whereas the rules that govern protein–

protein interactions are more complex. However, the sequence specificity and diversity of peptide-based materials affords the opportunity to introduce functional complexity, what has led to a more deeply exploration of the novo protein assemblies in the last years<sup>200</sup>.

Manmade self-assembling protein nanocages show highly ordered architecture with structural stability at the nano-scale and uniform size and shape distribution by self-assembly<sup>201</sup>. The construction of these assemblies relies on the controlled oligomerization of individual protein motifs or polypeptides, which act as building blocks of complex supramolecular arrangements<sup>183</sup>.

Existing **natural protein oligomerization motifs** have been recognized as suitable building blocks for the predictable bottom-up design of protein nanostructures<sup>202;203</sup>. Thus far, a variety of protein structural motifs can be used to promote and build larger protein structures in a self-assembled manner. These motifs can be collagen-mimetic peptides,  $\beta$ -sheet peptides and straight  $\alpha$ -helices. Beta-strands can interact forming amyloid fibrils<sup>204;205</sup> and gel-like structures<sup>206</sup>. In the case of  $\alpha$ -helices, their interaction results in adaptable coiled-coil structures<sup>207;208</sup>. Coiled-coil motifs, a structural motif in which 2-7  $\alpha$ -helices are coiled together like the strands of a rope, have been widely used for the generation of protein complexes such as nanofibres<sup>209</sup>, membranes<sup>210</sup>, nanotubes<sup>211</sup>, nanostructured films<sup>212</sup>, spherical structures<sup>213</sup> and responsive hydrogels<sup>214</sup>. As an example, homogeneous NPs with regular polyhedral symmetry, about 16 nm in diameter, were prepared from single type of polypeptide chains where the two coiled-coil modules with different oligomerization states were joined by a short linker<sup>215</sup>.

Unfortunately, these natural protein structural motifs display moderate functional versatility and so far, only few studies have investigated their role in nanomedicine.

In this context, the development of genetic engineering techniques has allowed the creation of **multifunctional self-assembling proteins**<sup>216-218</sup> with highly ordered architecture. Multifunctional proteins are manmade engineered chimerical molecules that present functional versatility achieved by genetic engineering and simple and cost effective biological production by recombinant systems (Figure 12).



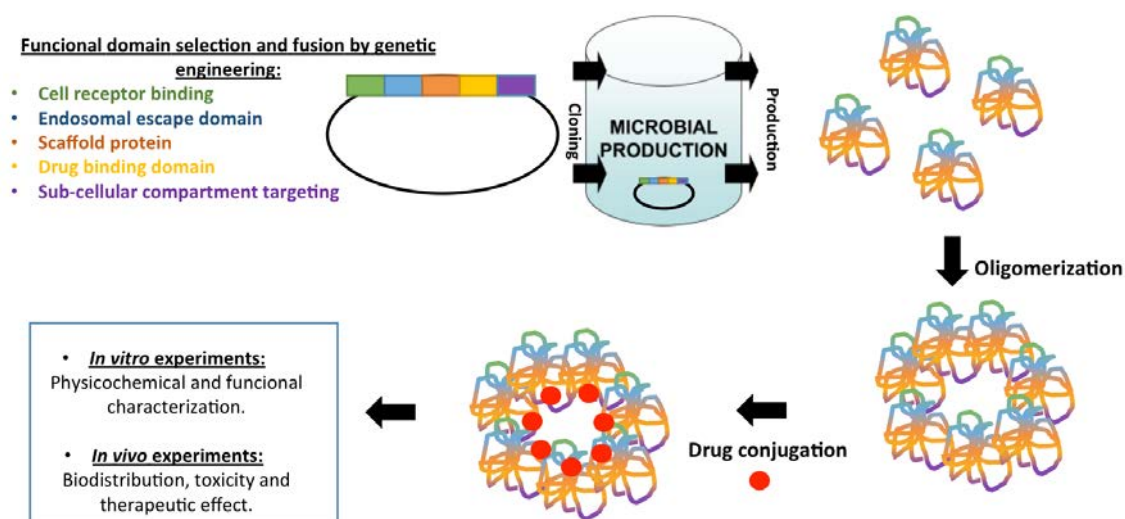


**Figure 12:** Schematic representation of the generation of recombinant multifunctional self-assembling drug-loaded protein nanoparticles.

### FUNCTIONAL VERSATILITY.

Functional versatility can be achieved by assembling different functional components required for effective drug delivery into a single chain polypeptide. The functional protein segments that are usually incorporated in these NPs include protein domains conferring oligomerization, systemic stability (protein scaffold), nucleic acid or drug interaction, cell targeting and internalization, endosomal escape, cytosolic mobility, nuclear localization or blood brain barrier crossing abilities<sup>216;219</sup>.

The formulation of the desired proteins as self-assembled protein only-NPs display targeting ligands, promotes the internalization into the cells and prevents renal filtration after in vivo administration of these proteins. Drugs can be chemically incorporated into the NPs by simple procedures.

### RECOMBINANT PROTEIN PRODUCTION.

Approximately 50 % of all new medicines are classified as recombinant biopharmaceuticals. There are more than 400 biopharmaceutical products in the market and other 1300 are undergoing clinical trials<sup>220</sup>.

The first system of choice for the production of recombinant proteins is *Escherichia coli*<sup>218;221</sup>. It has been successfully used to produce many proteins such as proinsulin,



growth hormone, interleukin, and antibody fragments. Human insulin was the first recombinant protein produced in *E. coli* in 1978 and approved by the FDA in 1982 for the treatment of diabetic patients.

The main advantages regarding recombinant protein production in this system involve its well-understood cell biology, its easy handling, the use of simple growth medium, its rapid cell growth, the simple fermentation process, the high product yields, the cost effective production, and its easy manipulation. The main drawback of it is the lack of post-translational modification<sup>222;223</sup>, loss of plasmid and antibiotic property<sup>221;224</sup>, improper protein refolding<sup>225;226</sup>, endotoxin issues due to the presence of lipopolysaccharide (LPS)<sup>227</sup>, and poor protein secretion<sup>228</sup>. Due to these limitations and depending on the produced protein, other production systems should be valued and selected<sup>229;230</sup> (Table 3).

**Table 3:** Comparison between recombinant protein production systems.

	<b>Bacteria</b>	<b>Yeast</b>	<b>Mammalian cells</b>	<b>Transgenic plants</b>	<b>Transgenic animals</b>
<b>Cost</b>	Cheap	Cheap	Expensive	Cheap	Expensive
<b>Distribution</b>	Feasible	Feasible	Difficult	Easy	Difficult
<b>Gene size</b>	Unknown	Unknown	Limited	Not limited	Limited
<b>Glycosylation</b>	Absent	Incorrect	Correct	Correct	Correct
<b>Production cost</b>	Medium	Medium	High	Medium	High
<b>Production scale</b>	Limited	Limited	Limited	Feasible	Limited
<b>Protein folding accuracy</b>	Low	Medium	High	High	High
<b>Protein homogeneity</b>	Low	Medium	Medium	High	High
<b>Protein yield</b>	Medium	High	Medium-high	High	High
<b>Safety</b>	Low	Unknown	Medium	High	High
<b>Scale up cost</b>	High	High	High	Low	High

The recent exploration of LPS-free systems for recombinant protein production such as endotoxin-free strains of *E. coli*<sup>227;231</sup> or gram positive bacteria<sup>232</sup> paves the road for a cost-efficient and versatile production of proteins intended for biomedical uses. This allows skipping endotoxin removal steps, gaining in biosafety and reducing production costs. Considering the limitation associated with the use of *E.coli* for protein production, an engineered strain with a modified LPS has been developed<sup>227</sup>. Specifically the engineered strain contains a non-decorated lipid IV<sub>A</sub> that lacks the acyl chains, decreasing the endotoxic response up to 95 %. Despite this strain has brought a quantum leap, there is still a lot to do to develop fully safe products to be accepted by the FDA in this system. On the other hand, gram positive bacteria such as *Bacillus*, *Corynebacterium* and Lactic acid bacteria, have been used for centuries in food production and preservation, being classified as food grade microorganisms<sup>232;233</sup>. They are Generally Recognized as Safe (GRAS) organisms by the FDA and fulfil criteria of the qualified presumption of safety (QPS) according to the European Food Safety Authority (EFSA). These bacteria have a peptidoglycan layer surrounding the cell membrane that does not contain LPS, thus, they are presented as very interesting alternative that may ensure the safety of the therapeutic proteins produced for biomedicine.

### HIGHLY ORDERED ARCHITECTURE.

The construction of these protein assemblies relies on the controlled oligomerization of individual multifunctional polypeptides, which act as building blocks of complex arrangements allowing the generation of self-assembled NPs.

Of course, the mentioned natural oligomerization domains can be incorporated into modular polypeptides to construct protein NPs based on hybrid fusion proteins acting as building blocks. However, the comprehension of the mechanics of the cross-molecular interactions that govern the formation of stable supramolecular complexes is still low.

Recently, a **new engineering oligomerization approach** has been developed in our research group which enables to obtain fully functional versatile NPs based on the combined use of non-amyloidogenic architectonic tags consisting in one cationic peptide plus a polyhistidine<sup>234;235</sup>. More in detail, the combination of a cationic peptide

at the amino terminus of a scaffold protein (i.e GFP or p53 proteins) with a poly-histidine tag at the carboxy terminus promotes the self-assembling of the building block in regular size NPs led by electrostatic interactions and followed by Van der Waals forces and hydrophobic bonding. Moreover, it has been shown that this self-assembly property is determined by the charge of the cationic peptide, being the size of the generated NPs proportional to the number of positive charges in each case<sup>235</sup> (Figure 13).

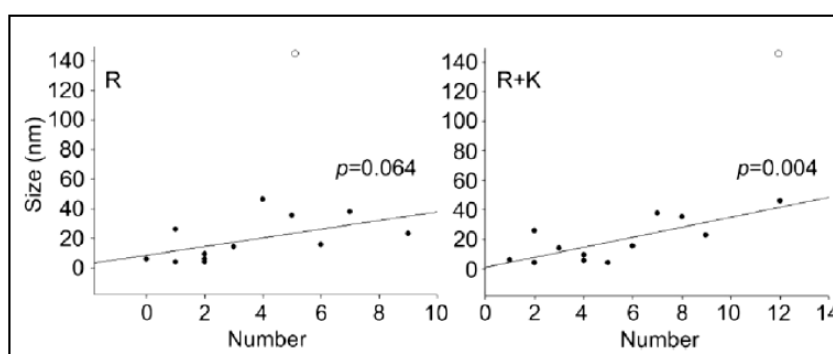


**Figure 13:** Regression analyses between different cationic peptides that have different number of positive charges and the size of the generated NPs. R stands for the number of arginine residues and R + K indicates the number of all cationic residues (arginines and lysines). The white symbol refers to data from CXCL12-empowered particles, and it has been excluded from the analyses. Figure obtained from <sup>235</sup>.

Interestingly, the N-terminal cationic peptide could act, in addition, as a cell-receptor specific ligand that confers targeting properties to the particle making these carriers very appealing as drug delivery systems<sup>236;237</sup>.

As an example, **T22-GFP-H6** is a fluorescent fusion protein that self-assembles as planar, cyclic homomeric NPs of 12 nm through the combination of electrostatic, hydrogen bond and Van der Waals forces<sup>234</sup>. This cationic peptide is an engineered version of polyphemusin II from Atlantic horseshoe crab *Limulus polyphemus*, that is a well-known antagonist of the cell surface CXCR4 over-expressed in metastatic colorectal cancer stem cells. These NPs have been designed for further conjugation with antitumoral drugs to selectively accumulate and internalize in CXCR4<sup>+</sup> cancer cells upon intravenous administration in CXCR4<sup>+</sup> CRC mice model<sup>234</sup>. This is expected to lead to selective DNA damage and apoptosis, and CXCR4<sup>+</sup> cell depletion within tumors.

### 3.2. PROTEIN ONLY NANOPARTICLES: CYTOTOXIC PROTEINS AS DRUGS.

The employment of many cytotoxic proteins as efficient drugs in DDS is a very attractive approach that allow excluding the need of drug conjugation and thus, the possibility of drug leakage<sup>238</sup> during circulation would be eliminated minimizing possible side effects.

Many proteins from diverse natural sources exhibit potent cytotoxic activities such as inhibition of enzymatic activities or by the cell cycle arrest, that can be used as drugs in DDS<sup>239-241</sup> (Table 4). Note that most of the cytotoxic proteins are not natural or modified versions, so they probably contain antigenic peptides that activate the immune system leading strong side effects and limiting their use in the clinic. Therefore, these proteins such as toxins and antibodies derivatives require deimmunization-oriented engineering and humanizing process respectively<sup>242</sup>. Deletion of the portions of these toxins that are not essential for cytotoxic activity or/and by eliminating antigenic T and B cell epitopes reduce the off-target effects. In this regard, **cytotoxic proteins from human origin** such as proapoptotic proteins and some antimicrobial peptides are imposed as very attractive and safe options as drugs.

The earliest strategies are based on simple fusion technologies that consist in the fusion of a cytotoxic protein to a cell-surface receptor ligand by chemical coupling. Immunotoxins (ITs) are the best representative example of these protein complexes and they are based on catalytic domains of plant or bacterial toxins fused to an antibody with selective targeting<sup>243</sup>. These fusions have proven to be really effective but show all the disadvantages described above for ADCs. As toxin components, *Pseudomonas* exotoxin (PE), diphtheria toxin (DT) and other ribosome-inactivating proteins such as ricin, saporin and gelonin, have been evaluated in clinical studies. ITs are able to kill tumor cells efficiently, but side-effects and immunogenicity have so far hampered their clinical breakthrough. Non-antibody protein agents as peptidic ligands or cell-penetrating peptides have been also fused to cytotoxic proteins but even though the specificity and internalization is enhanced, they still show inappropriate nanoscale size and therefore new approximations should be explored.

**Table 4:** Different cytotoxic proteins that can be used as drugs for DDS.

<b>CYTOTOXIC PROTEIN</b>	<b>ORIGIN</b>	<b>MECHANISM OF ACTION</b>	<b>EXAMPLES</b>
<b>Toxins or Venom components.</b>	Plants, microorganisms and amphibians.	Inhibition of protein translation, pore formation, cell cycle alterations among others.	Ricin, trichosantin, Diphtheria toxin, Pseudomonas aeruginosa exotoxin A, Chlorotoxin, Mellitin.
<b>Antimicrobial peptides.</b>	<b>Human</b> and other animals. Peptides libraries and the novo design.	Pore formation and cell lysis, anticancer activities (apoptosis, inhibition of tumor angiogenesis and immunomodulatory activities).	Cecropin, Defensin, Magainin, GWH1.
<b>Proapoptotic proteins.</b>	<b>Human</b>	Apoptosis.	Bak, PUMA, Bid, Bad.
<b>Antibodies.</b>	Human and other animals.	Inhibition of target receptor and immunomodulatory activities.	Anti-EGFR, Anti-VEGF.

In this context, we believe that modular design of smart cytotoxic proteins appears as very attractive approach that could allow the generation of multifunctional protein-only NPs with intrinsic cytotoxic activities. The incorporation of a functional cytotoxic protein as well as oligomerization domains, targeting agents and other functional domains discussed above into a single chain polypeptide, allow the generation of **“all-in-one” vehicle free protein therapeutic nanomedicines** for targeted drug delivery with an applicability in a variety of diseases.

## 4. OVERVIEW

Currently available conventional therapies are far from being fully effective; cancer therapies present high systemic toxicity and limited accessibility to metastatic foci<sup>64;90;92</sup>, being the formation of metastasis the main mortality cause<sup>60</sup>. The efficacy of antibiotics for infectious diseases has been hampered by the increasing incidence of multi-resistant bacterial infections<sup>115-117</sup>; and the blood–brain barrier (BBB) difficults the entry into the brain of most conventional drugs available for the treatment of brain diseases<sup>148;150</sup>. Therefore, the development of new nanomedicines is needed.

In this context, recombinant multifunctional self-assembling protein NPs are DDS that show high stability, biocompatibility, biodegradability, appropriate pharmacokinetics, specificity, efficient cell penetrability and they can be easily coupled with drugs showing high therapeutic effect<sup>216;219;234;235</sup>.

The novel oligomerization approach developed in our research group to generate these nanocarriers is based on cationic peptide and polyhistidine tail as oligomerization tags introduced in the building blocks by rational design. Conventional peptide drugs have low bioavailability when they are administered intravenously and the need to control nanoparticle size for their efficient biodistribution and delivery has been widely discussed in this introduction. Therefore, it is important to study how robust is our platform to its translational application.

Moreover, the high efficacy of this drug conjugated nanocarriers can be limited due to the possibility of drug leakage during circulation leading to side effects<sup>238</sup>. In this regard, we believe that modular design of cytotoxic proteins appears as very attractive approach to obtain “all-in-one” vehicle-free multifunctional protein therapeutic nanomedicines for targeted drug delivery with applicability in a variety of diseases.





## OBJECTIVES





The approach developed in our group is based on the application of a cationic protein region and a histidine tag as architectonic peptides that induce the oligomerization of multifunctional proteins into self-assembled NPs<sup>235;237</sup>. Moreover, when the cationic peptide is a ligand of a specific tumoral marker, these nanoscale materials show selective biodistribution and accumulation into the tumor upon intravenous administration<sup>234</sup>.

The aim of this thesis is to engineer cytotoxic proteins for the generation of “all-in-one” vehicle-free protein nanomedicines with intrinsic cytotoxic activities which have an applicability in a variety of diseases.

To this purpose, we planned the following objectives:

- 1) To evaluate the possibility of engineering pre-existing non cationic ligands into building blocks to promote their self-assembling in form of NPs and thus, explore the potency of this oligomerization approach for its broad applicability in nanomedicine.
- 2) To asses if the nanoparticulate presentation of multifunctional proteins favours their delivery to the brain and consider this protein oligomerization platform for its application in neurotropic therapy.
- 3) To generate CXCR4<sup>+</sup> targeted protein-only nanoparticles with intrinsic cytotoxic activities for the treatment of solid tumors.
- 4) To generate protein-only nanoparticles with intrinsic microbicide activities for bacterial infections treatment.





## RESULTS



## ARTICLE 1

### Rational engineering of single-chain polypeptides into protein-only, BBB-targeted nanoparticles.

**Naroa Serna**, María Virtudes Céspedes, Paolo Saccardo, Zhikun Xu, Ugutz Unzueta, Patricia Álamo, Mireia Pesarrodoná, Alejandro Sánchez-Chardi, Mónica Roldán, Ramón Mangués, Esther Vázquez, Antonio Villaverde and Neus Ferrer-Miralles.

**Nanomedicine: Nanotechnology, Biology, and Medicine.** 2016. 12: 1241–1251.

Impact factor: 5.720. Quartile: Q1. Decile: D1.

Formulating pre-existing proteins as nanoparticles would offer an interesting engineering tool with a broad applicability in nanomedicines. For instance, the precise sequence manipulation such as an increase in the cationic load of non cationic ligands could allow their incorporation as oligomerization tags into multifunctional proteins to promote their assembling into NPs. In this context, we could widely apply the described oligomerization platform to obtain any targeted NP suitable for nanomedicine.

As we have already demonstrated in colorectal cancer models, assembled as NPs and when empowered by homing peptides, these proteins correctly biodistribute and accumulate in target tissues. However, recent data suggest that the presentation of proteins in nanoparticulate entities might not favor protein delivery to brain, suggesting that brain targeting properties did not result improved by the multimerization.

In this work, we have engineered pre-existing non-cationic BBB homing peptides into building blocks and analyzed their performance as oligomerization tags (**objective 1**). Being their capability to form NPs successful, *in vitro* cell penetrability and *in vivo* biodistribution of both, disassembled and assembled versions have been examined to explore the utility of neurotropic protein-only NPs for treatment of CNS diseases (**objective 2**).





## Rational engineering of single-chain polypeptides into protein-only, BBB-targeted nanoparticles

Naroa Serna, BSc<sup>a,b,c</sup>, María Virtudes Céspedes, PhD<sup>c,d</sup>, Paolo Saccardo, PhD<sup>a,b,c</sup>,  
Zhikun Xu, PhD<sup>a,b,c</sup>, Ugutz Unzueta, PhD<sup>c,d</sup>, Patricia Álamo, PhD<sup>c,d</sup>,  
Mireia Pesarrodonà, BSc<sup>a,b,c</sup>, Alejandro Sánchez-Chardi, PhD<sup>e</sup>, Mónica Roldán, PhD<sup>e</sup>,  
Ramón Mangues, PhD<sup>c,d</sup>, Esther Vázquez, PhD<sup>a,b,c</sup>,  
Antonio Villaverde, PhD<sup>a,b,c,\*</sup>, Neus Ferrer-Miralles, PhD<sup>a,b,c,\*</sup>

<sup>a</sup>Institut de Biotecnologia i de Biomedicina, Universitat Autònoma de Barcelona, Bellaterra, Barcelona, Spain

<sup>b</sup>Departament de Genètica i de Microbiologia, Universitat Autònoma de Barcelona, Bellaterra, Barcelona, Spain

<sup>c</sup>CIBER de Bioingeniería, Biomateriales y Nanomedicina (CIBER-BBN), Bellaterra, Barcelona, Spain

<sup>d</sup>Oncogenesis and Antitumor Drug Group, Biomedical Research Institute Sant Pau (IIB-SantPau), Hospital de la Santa Creu i Sant Pau, Barcelona, Spain

<sup>e</sup>Servei de Microscòpia, Universitat Autònoma de Barcelona, Bellaterra, Barcelona, Spain

Received 10 April 2015; accepted 15 January 2016

### Abstract

A single chain polypeptide containing the low density lipoprotein receptor (LDLR) ligand Seq-1 with blood–brain barrier (BBB) crossing activity has been successfully modified by conventional genetic engineering to self-assemble into stable protein-only nanoparticles of 30 nm. The nanoparticulate presentation dramatically enhances *in vitro*, LDLR-dependent cell penetrability compared to the parental monomeric version, but the assembled protein does not show any enhanced brain targeting upon systemic administration. While the presentation of protein drugs in form of nanoparticles is in general advantageous regarding correct biodistribution, this principle might not apply to brain targeting that is hampered by particular bio-physical barriers. Irrespective of this fact, which is highly relevant to the nanomedicine of central nervous system, engineering the cationic character of defined protein stretches is revealed here as a promising and generic approach to promote the controlled oligomerization of biologically active protein species as still functional, regular nanoparticles.

© 2016 Elsevier Inc. All rights reserved.

**Key words:** Protein engineering; Nanoparticles; Self-assembling; Biodistribution; LDLR

The design and biofabrication of nanoscale materials that mimic viral properties (such as self-assembling, cell surface receptor binding, internalization and proper intracellular trafficking) are highly promising for targeted drug delivery and gene therapy.<sup>1</sup> Proteins are among the most convenient materials for the generation of functional building blocks in nanoparticle construction.<sup>2–5</sup> This is linked not only to protein functionalities but also to the fact that their spatial conformation, potential for cross-interactions and supramolecular organization can be designed and adjusted by simple genetic engineering. In addition, cost-effective biofabrication of proteins for therapeutic

applications has been fully demonstrated in Bio-Pharma, and the emergence of novel cell factories and the implementation of genetic and systems approaches expand the opportunities for the biosynthesis of difficult proteins.<sup>6–8</sup> Then, while protein production and downstream are technically solved issues, the bases for a rational engineering of protein–protein cross molecular interactions remain to be fully established.

Some architectonic principles have been proposed for the construction of peptide-based nanofibers and nanoparticles,<sup>4</sup> exploiting the amphiphilic character of chemically modified short peptides<sup>9</sup> or the self-assembling properties of the

The authors declare no competing interests. We are indebted to FIS PI12/01861, Marató 416/C/2013-2030 and NanoMets to RM, MINECO BIO2013-41019-P, AGAUR (2014SGR-132) and CIBER de Bioingeniería, Biomateriales y Nanomedicina (project NANOPROTHER) to AV for funding our research on protein-based therapeutics. Z.X. and M.P. acknowledge support from China Scholarship Council and Universitat Autònoma de Barcelona through pre-doctoral fellowships respectively.

\*Corresponding authors.

E-mail addresses: antoni.villaverde@uab.cat (A. Villaverde), neus.ferrer@uab.cat (N. Ferrer-Miralles).

<http://dx.doi.org/10.1016/j.nano.2016.01.004>

1549-9634/© 2016 Elsevier Inc. All rights reserved.



$\beta$ -sheet-rich amyloid protein domains.<sup>10</sup> In addition, the engineering of natural oligomerization domains into modular polypeptides has allowed the construction of protein nanoparticles based on hybrid fusion proteins acting as building blocks.<sup>11</sup> Of course, the production of structural viral proteins renders, in some cases, complex structures known as virus like particles (VLPs) that architecturally mimic the natural viral capsid versions. While largely proven to be excellent immunogens, the usability of VLPs and other nanostructured materials as vehicles for drug and nucleic acid delivery is rather narrow.<sup>12</sup> This is because of the limited versatility in the design of nanoscale physical properties and biological functions of the resulting nanoparticles, and on the other side, the still partial comprehension of the mechanics of the cross-molecular interactions that govern the formation of stable supramolecular complexes.

Recently, we have proposed a nanoscale architectonic principle that permits the generation of protein nanoparticles in which structurally unrelated protein species can act as building blocks.<sup>13</sup> When tagged with a cationic amino terminal peptide and a polyhistidine tail at the carboxy terminus, these scaffold proteins (eg. GFP, IRFP, p53 and Hsp 70), cross-interact by electrostatic interactions and form toroid structures stabilized by a complex set of alternative forces, including van der Waals and hydrogen bond interactions.<sup>14</sup> These nanoscale materials, of regulatable size, allow the intracellular delivery of functional proteins to specific target cells and tissues upon systemic administration.<sup>14–16</sup> In the form of nanoparticles and when conveniently empowered by tumor homing peptides, these proteins correctly biodistribute and accumulate, for instance, in CXCR4<sup>+</sup> cancer stem cells in colorectal cancer models.<sup>14</sup> However, recent indirect data suggested that the presentation of proteins as nanoparticulate entities might not favor protein delivery to brain.<sup>17</sup> This might be indicative of different principles governing the biodistribution of protein nanoparticles depending on if they display tumor- or BBB-homing peptides. To assess BBB-crossing and brain targeting properties of monomeric and nanoparticle versions of the same targeting peptide we have engineered for the first time, pre-existing BBB-homing polypeptides into building blocks that self-assemble as equivalent protein nanoparticles. Then, apart from determining the *in vitro* cellular penetrability, the biodistribution of both disassembled and assembled versions has been examined *in vivo* upon intravenous administration into healthy mice. Unexpectedly, while the cellular penetrability of protein nanoparticles is enhanced *in vitro* when compared to single molecular species, this is not accompanied by an enhanced ability of the protein to reach the brain. In addition to the protein engineering principles successfully tested here, the presented results indicate particular restrictions in nanoparticle performance in brain targeting, which should prompt the careful reconsideration of nanotechnological approaches to neurotropic vehicles for therapies and imaging.

## Methods

### Protein design and gene cloning

Angiopep-2 (TFFYGGSRGKRNNFKTEEY)<sup>18</sup> and Seq-1 (KYLAYPDSVHIW),<sup>19</sup> are peptides with known BBB-crossing activities that have been previously used to construct brain-

targeted GFP fusions. Derivatives of *Angiopep-2-GFP-H6* and *Seq-1-GFP-H6* containing additional cationic amino acids (Table 1) were designed in house and obtained from Genscript (Piscataway, USA). The synthetic genes (*Seq-1-7-GFP-H6*, *Seq-1-8-GFP-H6*, *Angiopep-2-7-GFP-H6* and *Angiopep-2-8-GFP-H6*) were then inserted into the prokaryotic expression commercial pET-22b vector (#69744-3, Novagen, USA) using *NdeI/HindIII* restriction sites. *Escherichia coli* BL21 (DE3) cells were transformed with recombinant pET22b plasmids by heat shock (45 s, 42 °C) to allow protein production.

### Protein production and purification

Bacterial cells carrying the appropriate plasmid vector were cultured in 2 L shaker flasks with 500 ml of LB (Luria-Bertani, Conda Cat. 1551.00) medium containing 100  $\mu$ g/ml ampicillin, at 37 °C until the OD<sub>550</sub> reached 0.5–0.7. Recombinant gene expression was induced with 0.1 mM isopropyl- $\beta$ -D-thiogalactopyronaside (IPTG) and then, bacterial cells were kept growing overnight at 20 °C. Bacterial cells were then harvested by centrifugation at 5000 g for 15 min at 4 °C and resuspended in Wash buffer (20 mM Tris-HCl, 500 mM NaCl, 10 mM imidazol, pH 8.0) PBS (phosphate buffered saline: 140 mM NaCl, 2.7 mM KCl, 10 mM Na<sub>2</sub>HPO<sub>4</sub>, 1.8 mM KH<sub>2</sub>PO<sub>4</sub>) in the presence of EDTA-free protease inhibitor (Complete EDTA-Free; Roche). Cells were then disrupted in a French Press (Thermo FA-078A) and centrifuged for 45 min (15,000 g at 4 °C). All proteins were purified by His-tag affinity chromatography using HiTrap Chelating HP 1 ml columns (GE healthcare) by ÄKTA purifier FPLC (GE healthcare). After filtering the soluble fraction, samples were loaded onto the column and washed with 10 column volumes of Wash buffer. Bound proteins were eluted with Elution buffer (20 mM Tris-HCl, 500 mM NaCl, 500 mM imidazole, pH 8.0) in a linear gradient. Purified fractions were collected and quantified by Bradford's assay and analyzed by SDS-PAGE and MALDI-TOF. The medium-scale production of recombinant proteins was partially performed by the ICTS "NANBIOSIS", more specifically by the Protein Production Platform of CIBER in Bioengineering, Biomaterials & Nanomedicine (CIBER-BBN)/IBB, at the UAB (SepBioEs, <http://www.nanbiosis.es/unit/u1-protein-production-platform-ppp/>).

### Microdialysis

Drops of purified proteins (20  $\mu$ l) were deposited on VsWp02500 Millipore membrane filters floating on 20 ml of different buffers: Carbonate buffer (166 mM NaHCO<sub>3</sub>, pH 7.5), Carbonate + dextrose 5% (166 mM NaHCO<sub>3</sub> pH 7.5 + 5% dextrose), Carbonate + salt (166 mM NaHCO<sub>3</sub> pH 7.5 + 200 mM NaCl) and HBS buffer 10 $\times$  (HEPES-buffered saline pH 5.8; 50 mM KCl, 1.37 M NaCl, 8.5 mM Na<sub>2</sub>HPO<sub>4</sub>, 21 mM HEPES).

Dialyzed drops were collected and centrifuged, and the soluble fractions were quantified to determine the extent of aggregation for each protein in different buffers. For further storage, proteins were finally dialyzed against their own most convenient buffer regarding protein stability (*Seq-1-7-GFP-H6* and *Seq-1-8-GFP-H6* against Carbonate buffer and *Angiopep-2-7-GFP-H6* and *Angiopep-2-8-GFP-H6* against Carbonate + 200 mM



Table 1  
Amino acid sequence of parental and engineered Angiopep-2-GFP-H6 and Seq-1-GFP-H6.

Name	Sequence <sup>b,c</sup>	MW (kDa)	Fluorescence intensity (%) <sup>d</sup>
Angiopep-2-7-GFP-H6 <sup>a</sup>	TFFYGGSRGKRN <sup><u>NFKTE</u></sup> EY- <b>RKR</b> -linker-GFP-HHHHHH	30.7	88
Angiopep-2-8-GFP-H6	TFFYGGSRGKRN <sup><u>NFKTE</u></sup> EY- <b>RKRK</b> -linker-GFP-HHHHHH	30.8	89
Seq-1-7-GFP-H6	<u>KYLA</u> YPDSVHIW- <b>RKRKRK</b> -linker-GFP-HHHHHH	30.5	51
Seq-1-8-GFP-H6	<u>KYLA</u> YPDSVHIW- <b>RKRKRKR</b> -linker-GFP-HHHHHH	30.6	52

<sup>a</sup> The nomenclatures 7 and 8 refer to the total number of cationic peptides resulting in the N-terminal segment.

<sup>b</sup> Underlined residues are the cationic amino acids already present in the original protein version. Bold segments correspond to the additional cationic peptides introduced in this study.

<sup>c</sup> The linker sequence is GGSSRSS.

<sup>d</sup> Specific fluorescence emission relative to that of GFP-H6 (238.9 U/mg).

NaCl buffer) and stored at  $-80^{\circ}\text{C}$  after 0.22 pore membrane filtration.

#### Fluorescence determination and dynamic light scattering (DLS)

Volume size distribution of nanoparticles and monomeric GFP protein fusions was determined by DLS at 633 nm (Zetasizer Nano ZS, Malvern Instruments Limited, Malvern, UK). Fluorescence was determined in a Varian Cary Eclipse fluorescence spectrophotometer (Agilent Technologies, Palo Alto, CA, USA) at 510 nm using an excitation wavelength of 450 nm.

For DLS analyses, proteins (stored at  $-80^{\circ}\text{C}$ ) were thawed and incubated on ice until use. 50  $\mu\text{l}$  of each sample was used in the corresponding stock concentration: Seq-1-7-GFP-H6: 2.67 mg/ml; Seq-1-8-GFP-H6: 2.2 mg/ml; Angiopep-2-7-GFP-H6: 3.93 mg/ml and Angiopep-2-8-GFP-H6: 2.58 mg/ml. For fluorescence determination, protein samples were diluted in the corresponding storage buffer to 0.5 mg/ml, in a final volume of 100  $\mu\text{l}$ . The shown data refer to the volume peak of the materials (the mode). For some experiments, protein samples were diluted to 1.5 mg/ml in reconstituted human plasma (Sigma-Aldrich, Ref: S225-5 ml), and further incubated under agitation at  $37^{\circ}\text{C}$ .

#### Electron microscopy (TEM and FESEM)

For transmission electron microscopy (TEM) two sets of purified proteins were diluted to 0.2–0.5 mg/ml, deposited onto carbon-coated copper grids (300 mesh) and one of them contrasted by uranyl acetate and air-dried and the other one shadowed with 1 nm a platinum-carbon layer respectively. Samples were observed in a Jeol 1400 transmission electron microscope operating at 80 kV and equipped with a CCD Gatan Erlangshen ES1000W camera. For field emission scanning electron microscopy (FESEM), microdrops of purified proteins diluted as for TEM were deposited onto a silicon wafer surface, air-dried and immediately observed in a Zeiss Merlin field emission scanning electron microscope operating at 1 kV and equipped with a high resolution in-lens secondary electron detector.

#### Cell culture and flow cytometry

LDLR<sup>+</sup> HeLa cells (ATCC-CCL-2) were used for the *in vitro* experiments. The cell line was cultured in Eagle's Minimum Essential Medium (Gibco, Rockville, MD) supplemented with

10 % fetal calf serum (Gibco), and incubated at  $37^{\circ}\text{C}$  and 5 %  $\text{CO}_2$  in a humidified atmosphere. Meanwhile bEnd.3 cell line was maintained in Dulbecco's Modified Eagle's Medium (DMEM: Gibco® GlutaMAX™) supplemented with 10 % fetal calf serum (Gibco), and incubated at  $37^{\circ}\text{C}$  and 10 %  $\text{CO}_2$  in a humidified atmosphere. Nanoparticles and proteins were added at different concentrations (ranging from 2 to 0.1 mM) to the cell culture in the presence of Optipro medium (Gibco) 24 h before flow cytometry. Cell samples were analyzed on a FACSCanto system (Becton Dickinson) using a 15 W air-cooled argon-ion laser at 488 nm excitation. GFP fluorescence emission was measured with a detector D (530/30 nm band pass filter) after treatment with 1 mg/ml trypsin (Gibco) for 15 min. For time course analysis, nanoparticles were added at 2 mM final to the cell culture in the presence of Optipro medium (Gibco) 24, 6, 4, 2 and 1 h, and 30 and 15 min before flow cytometry. Cell samples were analyzed after harsh treatment with 1 mg/ml trypsin (Gibco) for 15 min to remove surface attached fluorescent protein.<sup>20</sup>

#### Confocal microscopy

HeLa cells were grown on Mat-Teck culture dishes (Mat Teck Corporation, Ashland, MA). The nuclei were labeled with 10  $\mu\text{g}/\text{ml}$  Hoechst 33342 (Molecular Probes, Eugene, OR) and the plasma membranes with 5  $\mu\text{g}/\text{ml}$  CellMask™ Deep Red (Molecular Probes) in darkness for 10 min. Cells were washed in phosphate-buffered saline (Sigma-Aldrich Chemie GmbH, Steinheim, Germany) and proteins were added 20–24 h before staining at 2 mM. Live cells were recorded by TCS-SP5 confocal laser scanning microscopy (Leica Microsystems, Heidelberg, Germany) using a Plan Apo 63  $\times/1.4$  (oil HC  $\times$  PL APO lambda blue) objective. To determine the location of particles inside the cell, stacks of 10–20 sections were collected at 0.5  $\mu\text{m}$  Z-intervals with a pinhole setting of 1 Airy unit. The 3-D reconstruction was performed using Imaris software (Bitplane, Zürich, Switzerland).

#### Protein stability in human plasma

The stability of proteins was analyzed by measuring fluorescence emission after incubation in human plasma. Proteins were diluted, in triplicate, in human plasma (0.115  $\mu\text{g}/\mu\text{l}$  final concentration). Human plasma was obtained from a healthy donor in the Hospital de Sant Pau complying with

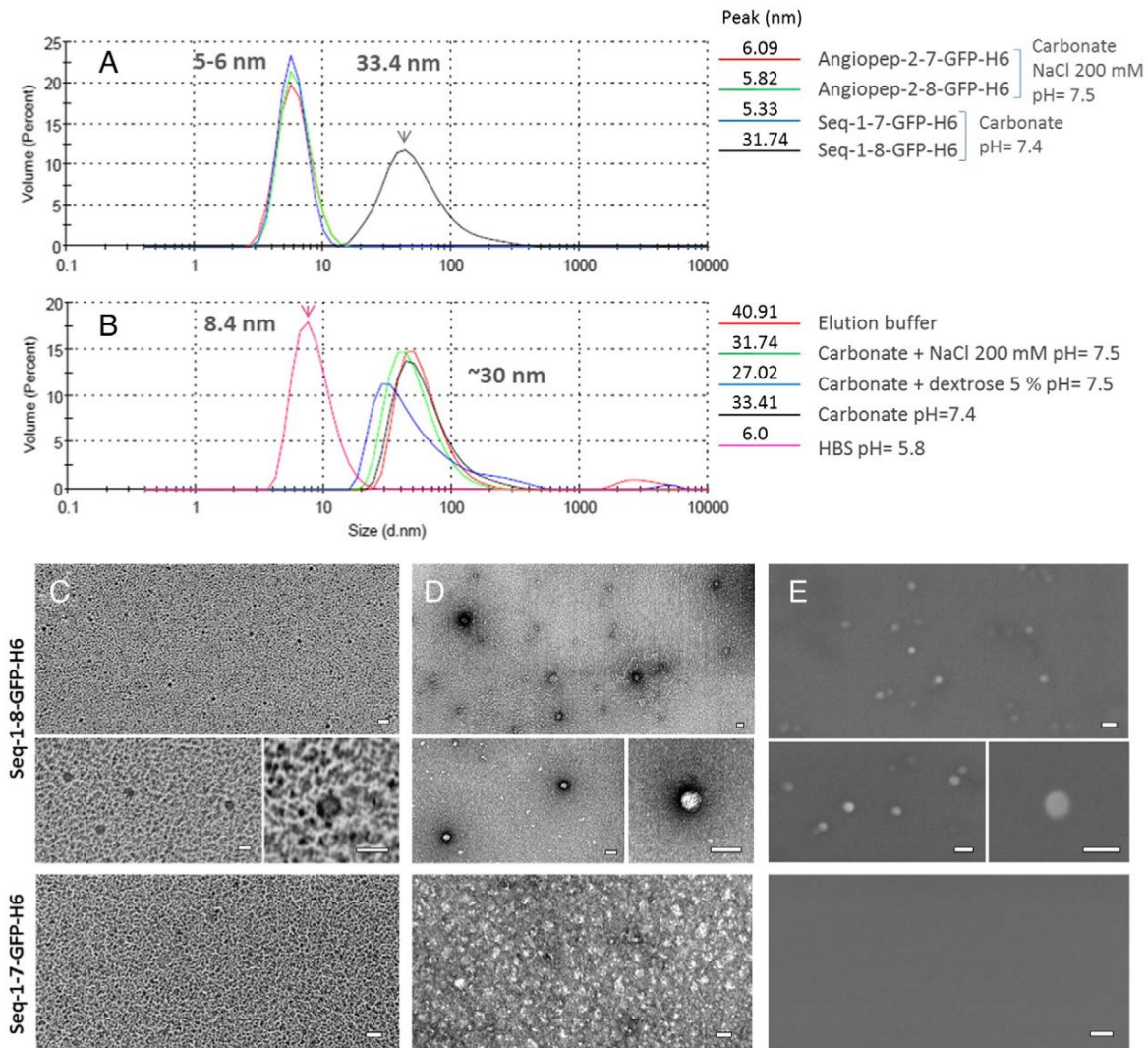


Figure 1. Formation and structure of Seq-1-8-GFP-H6 nanoparticles. (A) Size of Angiopep-2- and Seq-1-derived proteins measured by DLS in Carbonate buffer + 200 mM NaCl and Carbonate buffer respectively. The size of Seq-1-8-GFP-H6 nanoparticles is significantly different from the size of both Seq-1-7-GFP-H6 monomers and Angiopep-2 derivatives ( $P < 0.01$ ). (B) Stability of Seq-1-8-GFP-H6 nanoparticle in different physiological buffers. (C–D) Ultrastructural morphology of Seq-1-8-GFP-H6 nanoparticles at three different magnifications compared to the unassembled related protein Seq-1-7-GFP-H6 using shadowing of Pt/C (C) and negative staining (D) both with TEM, and deposition in silicon wafers for FESEM (E). Bar size is 50 nm.

the regulation established by the Clinical Ethics Committee of the Institution.

Immediately after dilution, samples were harvested (time 0) and their respective fluorescence was taken as the initial reference value (100%). Proteins were further incubated (at 37 °C, with agitation), and samples were taken, at different time points, up to 24 h. Protein functional stability during incubations was analyzed by fluorescence determination at 510 nm in a Cary Eclipse fluorescence spectrophotometer (Variant, Inc., Palo Alto, CA) using an excitation wavelength of 450 nm.

**Biodistribution**

Female athymic *nu/nu* mice (Charles River, L’Abresle, France) between 4 and 6 weeks of age were housed in

individually-ventilated cages on a 12-h light–dark cycle at 21–23 °C and 40–60% humidity. Mice were allowed free-access to an irradiated diet and sterilized water. The experimental animals received a single intravenous bolus of 500 µg of Seq-1-derived protein nanoparticles (or the equivalent unassembled proteins) in 166 mM carbonate buffer pH 7.5. Control animals received a single bolus of empty buffer. At 30 min and 2 h post-administration, we sacrificed the mice and measured *ex vivo* the amount of nanoparticles in each relevant organs from the experimental and control mice, by quantifying the emitted fluorescence. Entire hemisected organs (brain, kidney, liver, lung, heart) were placed in separate wells to detect the emitted signal using IVIS® Spectrum equipment (PerkinElmer Inc, Waltham, MA). The fluorescence signal was first digitalized, displayed as a pseudocolor overlay, and finally expressed as



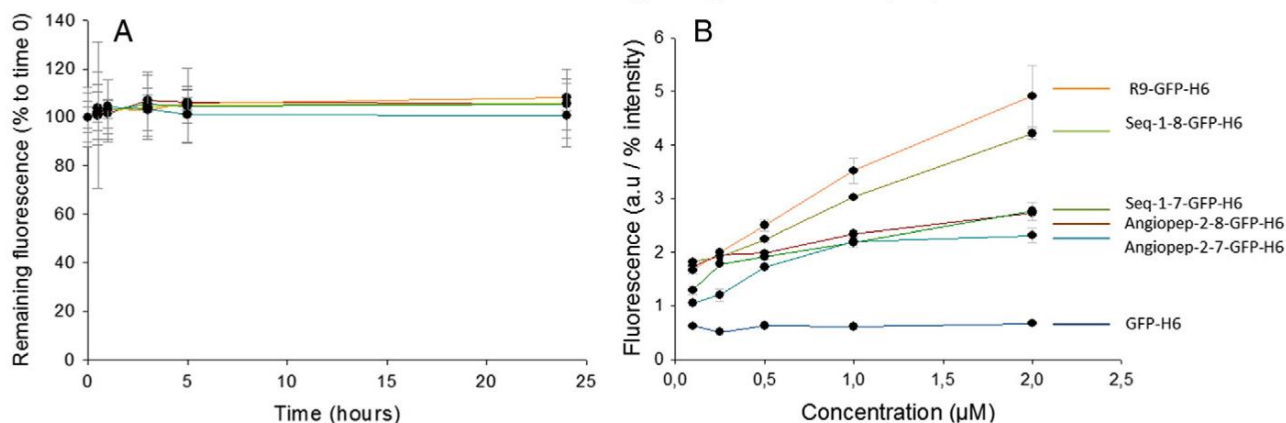


Figure 2. Biological characterization of modular proteins. (A) Time-dependent emission stability of protein constructs in human plasma. (B) Penetrability of the different protein constructs in cultured LDLR<sup>+</sup> HeLa cells, determined by flow cytometry upon harsh trypsin treatment.<sup>20</sup> Crude fluorescence values were corrected by the specific emission of each protein for comparative purposes. Data refer to 24 h post exposure.

radiant efficiency. Differences in signals were analyzed by a non-parametric Mann–Whitney test. The study was approved by the Hospital Sant Pau ethical committee and all procedures were in accordance with institutional guidelines. Humane care of the animals was always applied accordingly.

## Results

### Protein design, production and characterization

Angiopep-2-GFP-H6 and Seq-1-GFP-H6 are modular proteins displaying low density lipoprotein receptor (LDLR) ligands at their amino termini (Angiopep-2 and Seq-1 respectively) (Table 1), which reach the brain upon systemic administration.<sup>17</sup> Both Angiopep-2 and Seq-1 are well known BBB-crossing peptides proven useful as brain-homing agents in drug delivery.<sup>18,19</sup> Unlike the related construct ApoB-GFP-H6 that forms nanoparticles of 18 nm in diameter,<sup>17</sup> these proteins do not show any self-assembling activity and remain monomeric. In an attempt to upgrade Angiopep-2-GFP-H6 and Seq-1-GFP-H6 polypeptides up to self-assembling building blocks for nanoparticle construction, arginine- and lysine-containing stretches were designed for their introduction in both proteins, between the ligand and the linker to the scaffold GFP (Table 1, segments in bold). Two versions of the supplementary cationic peptides were constructed to offer a total of 7 or 8 positively charged residues in the amino terminal region. According to previous numerical modeling,<sup>15</sup> these numbers of cationic residues, if properly placed, should enable the proteins to self-organize as nanoparticles of around 30 nm. This numerical model identifies a relationship between the number of cationic residues at the amino terminus of the building blocks, and the size of the engendered particles, and it resulted from empirical data recruited from a set of different modular proteins. So far, the model had been never tested as a rational tool for the engineering of protein self-assembling.

The four new versions of Angiopep-2-GFP-H6 and Seq-1-GFP-H6 were produced in bacteria resulting in full-length

soluble species with predicted molecular masses (Table 1) and retaining the GFP fluorescence emission. The reduction of the fluorescence emission capacity, which is clearly significant ( $P < 0.01$ ) in the case of Seq-1-derivatives, is indicative of moderate conformational changes in the protein that while keeping the barrel organization might affect the conformation of the chromophore. While the parental versions are sized around 5–6 nm by DLS analysis, compatible with monomeric or dimeric GFP forms, the protein Seq-1-8-GFP-H6 was observed as nanoparticulate entities of around 30 nm, significantly different in size from unassembled monomers (Figure 1, A) and indicating a supramolecular organization of the individual polypeptide chains. The formed nanoparticles occurred and were stable in different buffers against which the protein was dialyzed (Figure 1, B), proving the structural robustness of the constructs under different salt contents and ionic strengths. In agreement, and fully supporting the taken approach to the engineering of building blocks, TEM and FESEM examinations confirmed the occurrence of these proteins as nanoparticles of regular size and morphology (Figure 1, C–E). Interestingly, high magnification TEM images of Seq-1-8-GFP-H6 showed an architectonic scheme (a circular electrodensity pattern) compatible with a toroid organization, similar to that recently shown for the related protein T22-GFP-H6.<sup>14</sup> This particular geometry was fully confirmed by high resolution FESEM analysis of the same samples (Figure 1, E). As expected, no nanoparticles but some unspecific aggregates with different shape and size were observed when examining Seq-1-7-GFP-H6 samples (Figure 1, C). As shown in Figure 1, A, none of the Angiopep-2-GFP-H6-derived proteins formed nanoparticles.

### In vitro analysis of cellular internalization

At this stage, we were interested in the biological characterization of Seq-1-8-GFP-H6 nanoparticles regarding their ability to penetrate target cells, and especially in comparison with the closely related, unassembled protein Seq-1-7-GFP-H6 that only differs by a single missing arginine residue (Table 1). Before

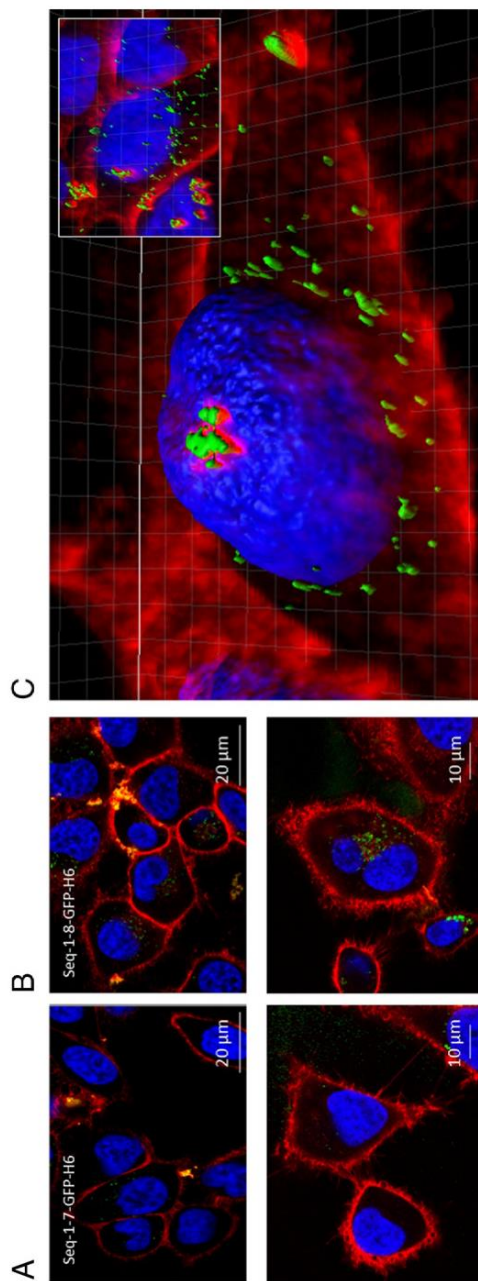


Figure 3. Internalization of protein constructs. Localization of protein Seq-1-7-GFP-H6 (A) and of Seq-1-8-GFP-H6 nanoparticles (B) upon 24 h of exposure to cultured HeLa cells, observed by fine confocal sections at two magnifications (top and bottom). Nuclear DNA is stained in blue, the membranous system in red, while nanoparticles and unassembled proteins are seen in green since they are naturally fluorescent. (C) Endosomal localization of Seq-1-8-GFP-H6 nanoparticles as observed by the yellowish merging of green and red signals in 3D confocal reconstructions.



Table 2  
*In vitro* transcytic capabilities of Seq-1-GFP-H6-derived proteins.

Construct	Concentration ( $\mu\text{M}$ )	Papp <sup>a</sup> (cm/s) $\times 10^{-6}$
Seq-1-7-GFP-H6	2.0	0.004 $\pm$ 0.01
	6.5	0.004 $\pm$ 0.002
Seq-1-8-GFP-H6	2.0	6.53 $\pm$ 0.001
	6.5	12.04 $\pm$ 0.01

<sup>a</sup> Papp: apparent permeability.

that, we determined that the fluorescence of Seq-1-8-GFP-H6 nanoparticles and of the whole set of unassembled proteins remained stable in human plasma *in vitro* at 37 °C for at least 24 h (Figure 2, A). The protein stability in presence of a complex organic medium prompted us to use fluorescence as a marker to monitor cell penetrability by flow cytometry, in LDLR-expressing HeLa cells. As observed (Figure 2, B), Seq-1-8-GFP-H6 penetrated HeLa cells much more efficiently than the closely related construct Seq-1-7-GFP-H6 and the monomeric versions of Angiopep-2-displaying proteins. Also, the levels of Seq-1-8-GFP-H6 internalization were comparable to those observed for the related R9-GFP-H6 nanoparticles used here as control, which are empowered by a potent Tat-inspired cell penetrating peptide (nine arginines, R9). R9 promotes receptor-independent fast cell penetrability and nuclear migration in HeLa and other cell types.<sup>21–23</sup> The similar uptake of Seq-1-8-GFP-H6 was indicative of an enhanced penetrability of the Seq-1 ligand when organized in a nanoparticulate form. Confocal images of HeLa cells exposed to Seq-1-derived proteins confirmed the poor penetrability of Seq-1-7-GFP-H6 (Figure 3, A) and the intracellular location of Seq-1-8-GFP-H6 (Figure 3, B), discarding mere external association to the cell membrane. Also, 3D reconstructions of exposed cultures resulted in images compatible with the expected endosomal route for Seq-1-8-GFP-H6 uptake, based on the merging of red (membranes) and green (nanoparticles) signals (Figure 3, C).

To evaluate if the enhanced cell internalization of Seq-1-8-GFP-H6 (in comparison to Seq-1-7-GFP-H6) would impact on the BBB-crossing abilities of Seq-1 we first tested both proteins in a CaCo-2 cell permeability system recognized as a relevant *in vitro* model of the BBB.<sup>24</sup> In this test, Seq-1-8-GFP-H6 showed transcytic properties clearly superior to those exhibited by Seq-1-7-GFP-H6 (Table 2), again in the line of the higher cell penetrability of a nanoparticulate version of the homing peptide Seq-1.

#### Biodistribution and BBB-crossing

When administered intravenously in healthy mice models with intact BBB, both Seq-1-7-GFP-H6 and Seq-1-8-GFP-H6 transiently accumulated in brain (Figure 4, A), over the background values derived from GFP-H6 administration (Figure 5, B). Despite being more efficient in cell penetration *in vitro* (Figures 2 and 3, and Table 2), the nanoparticulate version of Seq-1, namely Seq-1-8-GFP-H6, did not show any improvement of CNS targeting regarding the unassembled Seq-1-7-GFP-H6 form. On the other hand, none of these proteins were found in liver, heart and lung (Figure 5, A). The occurrence in kidney was not unforeseen in the cases of GFP-H6 and the unassembled Seq-1-7-GFP-H6, which are cleared by renal glomeruli. However, Seq-1-8-GFP-H6

nanoparticles would be expected to escape from renal filtration and occur only in target organs, as observed in the case of similar constructs functionalized with tumor-homing peptides.<sup>15</sup> This could be indicative of a partial disassembling of Seq-1-8-GFP-H6 nanoparticles *in vivo*, due to the high ionic strength and the presence of a complex spectrum of interacting human proteins, and a consequent reduction of the Seq-1-8-GFP-H6 material size from 30 nm (nanoparticles) to less than 8 nm (unassembled building blocks). While this does not occur in the case of the structurally related, more cationic T22-IRFP-H6 nanoparticle,<sup>14</sup> which is fully stable during circulation in blood, it would be not unexpected in the case of the less cationic Seq-1-8-GFP-H6, since the absence of one single lysine (in Seq-1-7-GFP-H6) precludes self-assembling. To check this possibility, we explored *in vitro* the nanoparticle stability in presence of human sera, at 37 °C, to mimic post injection conditions. As observed (Figure 5, B), Seq-1-8-GFP-H6 nanoparticles lost stability with incubation time, showing a moderate reduction of size at 2 h and being essentially disassembled at 5 h. Partial *in vivo* disassembly at 2 h would, at least to some extent, account for the presence of the material in kidney. However, while the amount of monomeric GFP-H6 and Seq-1-7-GFP-H6 dramatically decreased from 30 min to 2 h post administration, as expected for materials  $\leq 8$  nm in size, Seq-1-8-GFP-H6 nanoparticles remained in kidney for longer times (Figure 5, C). This fact suggested issues additional to size-dependent filtration as contributors in regulating its occurrence in kidney.

#### Discussion

By using empirical information from of a set of closely related proteins with and without self-assembling properties,<sup>25</sup> we have designed and constructed protein-only nanoparticles containing the Seq-1 BBB-crossing peptide (Figure 1). This has been done by the addition of several cationic peptides at the amino terminus of the modular protein Seq-1-GFP-H6 (Table 1), a polypeptide that exclusively remains in unassembled form (Figure 1). A similar attempt to engineer the self-assembling of Angiopep-2-GFP-H6 failed (Figure 1) probably because of the more scattered distribution of cationic residues (Table 1). This would result in a less polar splitting of the electrostatic charges necessary for the assembling of building blocks.<sup>13–15</sup> In fact, one additional cationic lysine residue in Seq-1-8-GFP-H6 compared to Seq-1-7-GFP-H6 was sufficient to efficiently triggering self-assembling (Table 1, Figure 1). Seq-1-8-GFP-H6 nanoparticles exhibited the expected size of 30 nm (Figure 1, A), a toroid organization (Figure 1, C and E) and a higher cellular penetrability into LDLR<sup>+</sup> HeLa cells when compared with the unassembled Seq-1-7-GFP-H6 version (Figures 2 and 3). In addition, the transcytic properties of Seq-1-8-GFP-H6, measured in a CaCo-2-based test,<sup>24</sup> were clearly superior to those exhibited by the unassembled form Seq-1-7-GFP-H6 (Table 2). Since the mere addition of cationic peptides to pre-existing protein nanoparticles did not alter cell penetrability *per se*,<sup>26</sup> the formation of nanoparticles rather than the single amino acid addition in Seq-1-8-GFP-H6 would be responsible for enhanced cell penetrability. A higher



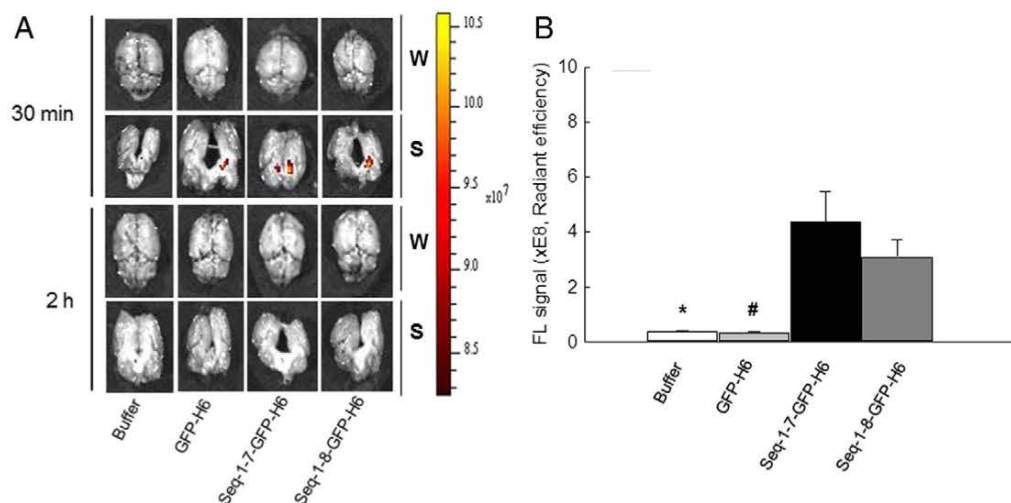


Figure 4. Brain targeting of Seq-1-derived proteins upon systemic administration at 500  $\mu\text{g}$  dose. (A) BBB-crossing registered ex vivo by GFP fluorescence determination in mouse whole brain (W) and brain sections (S) 30 min and 2 h after intravenous administration. Crude fluorescence values were corrected by the specific emission of each protein for comparative purposes. (B) GFP fluorescence values in brain sections. Data are normalized by the specific fluorescence. The scale and fluorescence signal values are expressed as Radiant efficiency [ $\text{p/s/cm}^2/\text{sr}$ ]  $\mu\text{W/cm}^2$ . Those groups showing significant differences with the rest of the groups are labeled with symbols (\*, #  $P < 0.05$ ).

penetrability of protein nanoparticles compared with individual building blocks is in agreement with previous results obtained in our laboratory<sup>17</sup> and it is probably related with the multivalent presentation of the cell ligands (Seq-1, in the present case) on the surface of nanoparticles that favors endosomal entrapment.<sup>27</sup> The endosomal route of Seq-1-8-GFP-H6 nanoparticle uptake is confirmed by the strong merging signals (yellowish spots, merging green and red) observed in *in vivo* internalization assays (Figure 3, B and C). Of course, the mere enlargement of the material size associated to oligomerization might also promote endocytosis, as size of nanoparticles generically determines the nature of cell responses upon exposure, including signaling and endocytosis.<sup>28</sup> Among nanoparticles between 2 and 100 nm, those sized between 40 and 50 nm show the strongest effect on cell responses, representing a size range compatible with what has been generically found as optimal for cell internalization in other independent studies.<sup>29–31</sup>

Despite the dramatic improvement of cell penetrability and transcytosis exhibited by the nanoparticulate versus free form of Seq-1 homing peptide, the accumulation in brain of Seq-1-7-GFP-H6 and Seq-1-8-GFP-H6 was similar and indistinguishable (Figure 4). This fact indicates that the multivalent presentation of the Seq-1 LDLR ligand in organized nanoparticles has no relevant impact on BBB permeability in healthy animals. This is in agreement with recent data<sup>17</sup> regarding the poor brain penetrability of nanoparticles empowered with the BBB-crossing peptide ApoB,<sup>32</sup> and it could be due to different transcytosis activities between epithelial kidney cells and brain endothelial cells, as previously described for a different receptor.<sup>33</sup>

On the other hand, both Seq-1-7-GFP-H6 and Seq-1-8-GFP-H6 were found in kidney (but not in other organs), as in the case of the parental protein GFP-H6 (Figure 5, A). This could be interpreted by assuming an imperfect stability of

Seq-1-8-GFP-H6 nanoparticles that might (at least partially) disassemble once in the blood stream. In fact, *in vivo* disassembling of protein nanoparticles is not totally unexpected since it has been already described that nab-paclitaxel nanoparticles (known as Abraxane and sized 130 nm), which are fully stable in physiological buffers and in saline solution, quickly separated into individual albumin-paclitaxel complexes once injected into the blood stream.<sup>34</sup> In this context, Seq-1-8-GFP-H6, which exhibited the same size (30 nm) in human sera than in buffer (Figure 1), appeared only as partially stable in sera under prolonged incubation (Figure 5, B), as a reduction of particle size was observed after 2 h of incubation and a significant occurrence of monomers at 5 h, a later time point than those considered for biodistribution analyses (30 min and 2 h). On the other hand, the presence of heterologous proteins in human sera would also promote, at least at some extent, structural or functional instability of the material by the presence of the corona.<sup>35</sup> However, the dynamic analyses of the renal occurrence of the proteins analyzed here (Figure 5, C) show clear and significant differences when comparing the monomeric versions (GFP-H6 and Seq-1-7-GFP-H6) and the multimeric form Seq-1-8-GFP-H6. This last protein remains for a longer time in kidney, suggesting that in addition to a potential size-dependent renal filtration of part of the material, its occurrence in the tissue might rely on a specific interaction between Seq-1 and tissue specific receptors such as megalin. Megalin, a cell surface receptor of the LDLR family found in renal cell types, participates in lipid metabolism in the kidney,<sup>36</sup> showing a high capacity for taking up lipid-binding proteins into the renal proximal tubule epithelial cells where it is highly expressed.<sup>37</sup> It is known that protein uptake by the proximal tubules is the main process ensuring the lack of proteins in urine. Moreover, since it occurs distally to glomerular filtration, only proteins of a size lower than the filtration cut-off (8 nm) can be taken

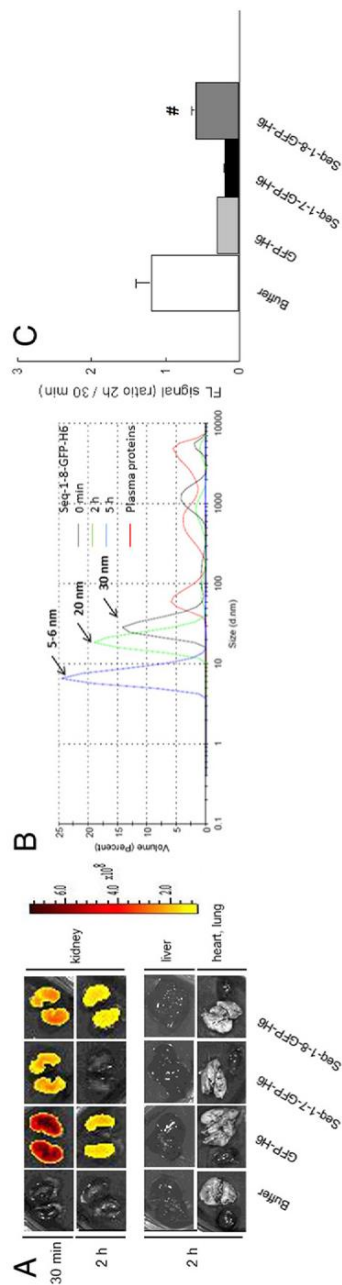


Figure 5. Renal clearance and biodistribution of Seq-1-derived proteins upon systemic administration of 500  $\mu\text{g}$ . (A) *Ex vivo* determination of GFP fluorescence signal in kidneys and other relevant organs such as livers, hearts and lungs, at the same post-injection times. Crude fluorescence values were corrected by the specific emission of each protein for comparative purposes. (B) Size variation of Seq-1-8-GFP-H6 materials during incubation in human plasma. (C) GFP fluorescence values in kidney sections. Data are normalized by the specific fluorescence. The scales and fluorescence signal measures are expressed as Radiant efficiency [ $\text{p/s/cm}^2/\text{sr}$ ]  $\mu\text{W/cm}^2$ . Those groups showing significant differences with the rest of the groups are labeled with symbols ( $\# p < 0.05$ ).



up.<sup>38</sup> Despite this, some receptor expression might occur in the endothelia of the glomerulus, accounting for a certain level of specific binding of nanomaterials over 8 nm. Although this hypothesis would obviously need further solving, the abundance of LDLR in kidney might discourage the use of LDLR ligands in nanoparticles targeted to brain, especially if they occur in sizes close to the renal cut-off.

In this study, we have engineered the brain-targeted polypeptide Seq-1-GFP-H6 to self-assemble into regular, protein-only nanoparticles formed by multiple copies of the resulting protein Seq-1-8-GFP-H6. Seq-1-8-GFP-H6 differs from the parental protein by 7 cationic residues that were inserted into a permissive region of the protein, between the Seq-1 peptide and the core GFP (Table 1). The resulting fluorescent nanoparticles show a dramatic improvement of cell penetrability and transcytic activities *in vitro* regarding monomeric versions, but contrarily, the brain targeting properties did not result improved by the multimerization (Figure 4). The engineering principle developed here should permit the construction of protein-based nanoparticles by the precise sequence manipulation of pre-existing proteins that increase, in a controlled way, the cationic load of the amino terminal regions. Also, the progressive developments in systems and genetic approaches to recombinant protein production<sup>39</sup> increasingly facilitate protein engineering, biofabrication in cell factories<sup>40</sup> and downstream.<sup>40,41</sup> In the current bubbling context of novel protein drugs of interest in cancer therapies and for other conditions,<sup>42,43</sup> formulating such therapeutic proteins as nanoparticles would offer an interesting engineering tool with a broad applicability in nanomedicine, as the multivalent presentation of homing agents in those materials, either natural or added, is expected to dramatically enhance cell uptake.

### Acknowledgments

The authors acknowledge the ICTS “NANBIOSIS”, more specifically by the Protein Production Platform of CIBER in Bioengineering, Biomaterials & Nanomedicine (CIBER-BBN)/IBB, at the UAB (SepBioEs, <http://www.ciber-bbn.es/en/programas/89-plataforma-de-produccion-de-proteinas-ppp>). We thank the CIBER-BBN Nanotoxicology Unit for fluorescent *in vivo* follow-up using the IVIS equipment. We are also indebted to the Cell Culture and Cytometry Units of the Servei de Cultius Cellulars, Producció d'Anticossos i Citometria (SCAC), and to the Servei de Microscòpia, both at the UAB, and to the Soft Materials Service (ICMAB-CSIC/CIBER-BBN). AV received an ICREA ACADEMIA award.

### References

- Mastrobattista E, et al. Artificial viruses: a nanotechnological approach to gene delivery. *Nat Rev Drug Discov* 2006;**5**:115-21.
- Elsadek B, Kratz F. Impact of albumin on drug delivery—new applications on the horizon. *J Control Release* 2012;**157**:4-28.
- Ferrer-Miralles Neus, et al. Engineering protein self-assembling in protein-based nanomedicines for drug delivery and gene therapy. *Crit Rev Biotechnol* 2015;**35**:209-21.
- Corchero JL, et al. Recombinant protein materials for bioengineering and nanomedicine. *Nanomedicine (Lond)* 2014;**9**:2817-28.
- Desa N. Challenges in development of nanoparticle-based therapeutics. *AAPS J* 2012;**14**:282-95.
- de Marco A. Recombinant polypeptide production in *E. coli*: towards a rational approach to improve the yields of functional proteins. *Microb Cell Fact* 2013;**12**:101.
- Ferrer-Miralles N, Villaverde A. Bacterial cell factories for recombinant protein production; expanding the catalogue. *Microb Cell Fact* 2013;**12**:113.
- Mahalik S, et al. Genome engineering for improved recombinant protein expression in *Escherichia coli*. *Microb Cell Fact* 2014;**13**:177.
- Cui H, et al. Self-assembly of peptide amphiphiles: from molecules to nanostructures to biomaterials. *Biopolymers* 2010;**94**:1-18.
- Gazit E. Self-assembled peptide nanostructures: the design of molecular building blocks and their technological utilization. *Chem Soc Rev* 2007;**36**:1263-9.
- Ren D, et al. Protein nanocapsules containing doxorubicin as a pH-responsive delivery system. *Small* 2011;**7**:1051-60.
- Ramqvist T, Andreasson K, Dalianis T. Vaccination, immune and gene therapy based on virus-like particles against viral infections and cancer. *Expert Opin Biol Ther* 2007;**7**:997-1007.
- Unzueta U, et al. Non-amyloidogenic peptide tags for the regulatable self-assembly of protein-only nanoparticles. *Biomaterials* 2012;**33**:8714-22.
- Céspedes MV, et al. In vivo architectonic stability of fully de novo designed protein-only nanoparticles. *ACS Nano* 2014;**8**:4166-76.
- Pesarrodona M, et al. Intracellular targeting of CD44 cells with self-assembling, protein only nanoparticles. *Int J Pharm* 2014;**473**:286-95.
- Unzueta U, et al. Intracellular CXCR4<sup>+</sup> cell targeting with T22-empowered protein-only nanoparticles. *Int J Nanomedicine* 2012;**7**:4533-44.
- Xu, et al. Targeting low-density lipoprotein receptors with protein-only nanoparticles. *J Nanoparticle Res* 2015;**17**:150.
- Demeule M, Currie JC, Bertrand Y, Ché C, Nguyen T, Régina A, et al. Involvement of the low-density lipoprotein receptor-related protein in the transcytosis of the brain delivery vector angiopep-2. *J Neurochem* 2008;**106**:1534-44.
- Maggie JM. *Peptide for transmigration across blood brain barrier and delivery systems comprising the same*. United States Patent Application Publication US 2011/0165079 A1; 2011.
- Richard JP, et al. Cell-penetrating peptides. A reevaluation of the mechanism of cellular uptake. *J Biol Chem* 2003;**278**:585-90.
- Madani F, Lindberg S, Langel U, Futaki S, Gräslund A. Mechanisms of cellular uptake of cell-penetrating peptides. *J Biophys* 2011:414729.
- Fuchs SM, Raines RT. Pathway for polyarginine entry into mammalian cells. *Biochemistry* 2004;**43**:2438-44.
- Vazquez E, et al. Protein nanodisk assembling and intracellular trafficking powered by an arginine-rich (R9) peptide. *Nanomedicine (Lond)* 2010;**5**:259-68.
- Hellinger E, et al. Comparison of brain capillary endothelial cell-based and epithelial (MDCK-MDR1, Caco-2, and VB-Caco-2) cell-based surrogate blood–brain barrier penetration models. *Eur J Pharm Biopharm* 2012;**82**:340-51.
- Unzueta U, et al. Non amyloidogenic arginine-rich peptide tags for the tailored self-assembling of protein nanoparticles. *Biomaterials* 2012;**33**:8714-22.
- Unzueta U, et al. Improved performance of protein-based recombinant gene therapy vehicles by tuning downstream procedures. *Biotechnol Prog* 2013;**29**:1458-63.
- Unzueta U, et al. Towards protein-based viral mimetics for cancer therapies. *Trends Biotechnol* 2015;**33**:253-8.
- Jiang W, Kim B, Rutka JT, Chan WCW. Nanoparticle-mediated cellular response is size-dependent. *Nat Nanotechnol* 2008;**3**:145-50.
- Shang L, Nienhaus K, Nienhaus GU. Engineered nanoparticles interacting with cells: size matters. *J Nanobiotechnol* 2014;**12**:5.
- Rejman J, Oberle V, Zuhom IS, Hoekstra D. Size-dependent internalization of particles via the pathways of clathrin- and caveolae-mediated endocytosis. *Biochem J* 2004;**377**:159-69.
- Shilo M, et al. The effect of nanoparticle size on the probability to cross the blood–brain barrier: an in-vitro endothelial cell model. *J Nanobiotechnol* 2015;**13**:19.
- Spencer BJ, Verma IM. Targeted delivery of proteins across the blood–brain barrier. *Proc Natl Acad Sci U S A* 2007;**104**:7594-9.
- Su T, Stanley KK. Opposite sorting and transcytosis of the polymeric immunoglobulin receptor in transfected endothelial and epithelial cells. *J Cell Sci* 1998;**111**:1197-206.

34. Bhardwaj V, Ravi-Kumar MNV. Drug delivery systems to fight cancer. In: Siepmann Juergen, Siegel Ronald A, Rathbone Michael J, editors. *Fundamentals and applications of controlled release drug delivery Advances in delivery science and technology* 978-1-4614-0880-2; 2012. p. 493-516. [Chapter 15].
35. Salvati, et al. Transferrin-functionalized nanoparticles lose their targeting capabilities when a biomolecule corona adsorbs on the surface. *Nat Nanotechnol* 2013;**8**:137-43.
36. Moestrup SK, Nielsen LB. The role of the kidney in lipid metabolism. *Curr Opin Lipidol* 2005;**16**:301-6.
37. Christensen EI, et al. Receptor-mediated endocytosis in renal proximal tubule. *Pflugers Arch* 2009;**458**:1039-48.
38. Bertrand N, Leroux JC. The journey of a drug-carrier in the body: an anatomo-physiological perspective. *J Control Release* 2012;**161**:152-63.
39. de Marco A. Strategies for successful recombinant expression of disulfide bond-dependent proteins in *Escherichia coli*. *Microb Cell Fact* 2009;**8**:26.
40. Vazquez E, Villaverde A. Microbial biofabrication for nanomedicine: biomaterials, nanoparticles and beyond. *Nanomedicine (Lond)* 2013;**8**:1895-8.
41. Singh A, et al. Solubilization and refolding of inclusion body proteins. *Methods Mol Biol* 2015;**1258**:283-91.
42. Mamat U, et al. Detoxifying *Escherichia coli* for endotoxin-free production of recombinant proteins. *Microb Cell Fact* 2015;**14**:57.
43. Guillard S, et al. Engineering therapeutic proteins for cell entry: the natural approach. *Trends Biotechnol* 2015;**33**:163-71.



## ARTICLE 2

### Peptide-Based Nanostructured Materials with Intrinsic Proapoptotic Activities in CXCR4<sup>+</sup> Solid Tumors.

**Naroa Serna**, María Virtudes Céspedes, Laura Sánchez-García, Ugutz Unzueta, Rita Sala, Alejandro Sánchez-Chardi, Francisco Cortés, Neus Ferrer-Miralles, Ramón Mangues, Esther Vázquez, and Antonio Villaverde.

**Advanced Functional Materials. 2017. 27, 1700919.**  
Impact factor: 12.124. Quartile: Q1. Decile: D1.

The systemic administration of chemical drugs in form of nanoconjugates benefits from enhanced drug stability when compared to free molecules, increasing the therapeutic impact and benefits for the patient.

However, many protein species are themselves, efficient drugs usable in human therapy such as human proapoptotic proteins, antimicrobial peptides or toxins.

The engineering of recombinant protein drugs as self-organizing building blocks of protein only nanoparticles would allow to obtain fully biocompatible and biodegradable nanomaterials that act as nanoscale drugs and show intrinsic therapeutic activities. This would allow the biological production in a single step of the nanoscale protein materials, excluding the need of further activation and drug conjugation and eliminating the possibility of drug leakage during circulation.

In this work, we have conducted a successful proof of concept, engineering three proapoptotic peptides to self-assemble as CXCR4-targeted protein only nanoparticles for the treatment of colorectal cancer (**objective 3**).





# Peptide-Based Nanostructured Materials with Intrinsic Proapoptotic Activities in CXCR4<sup>+</sup> Solid Tumors

Naroa Serna, María Virtudes Céspedes, Laura Sánchez-García, Ugutz Unzueta, Rita Sala, Alejandro Sánchez-Chardi, Francisco Cortés, Neus Ferrer-Miralles, Ramón Mangues,\* Esther Vázquez, and Antonio Villaverde\*

Protein materials are gaining interest in nanomedicine because of the unique combination of regulatable function and structure. A main application of protein nanoparticles is as vehicles for cell-targeted drug delivery in the form of nanoconjugates, in which a conventional or innovative drug is associated to a carrier protein. Here, a new nanomedical approach based on self-assembling protein nanoparticles is developed in which a chemically homogeneous protein material acts, simultaneously, as vehicle and drug. For that, three proapoptotic peptidic factors are engineered to self-assemble as protein-only, fully stable nanoparticles that escape renal clearance, for the multivalent display of a CXCR4 ligand and the intracellular delivery into CXCR4<sup>+</sup> colorectal cancer models. These materials, produced and purified in a single step from bacterial cells, show an excellent biodistribution upon systemic administration and local antitumoral effects. The design and generation of intrinsically therapeutic protein-based materials offer unexpected opportunities in targeted drug delivery based on fully biocompatible, tailor-made constructs.

## 1. Introduction

The systemic administration of drugs in form of nanoconjugates benefits from enhanced drug stability when compared to free molecules.<sup>[1]</sup> Valuable additional properties such as cell-targeting might also be merged into a given hybrid composite through the chemical incorporation of functional groups in nanoscale vehicles, taking profit from the high surface/volume

ratio of nanomaterials.<sup>[2]</sup> When administered systemically, the resulting drug-loaded conjugates sizing between ≈8 and 100 nm escape from renal filtration in absence of aggregation in lung or other highly vascularized organs.<sup>[3]</sup> This fact, combined with appropriate physicochemical properties of the material might result in extended circulation time and prolonged drug exposure to target organs, thus enhancing the therapeutic impact and benefits for the patient. Among the diversity of materials under investigation as drug carriers, including metals, ceramics, polymers, and carbon nanotubes, proteins offer unique properties regarding biocompatibility and degradability, that in the context of rising nanotoxicological concerns,<sup>[4]</sup> make them especially appealing. As the engineering of protein self-assembling into nanostructured materials is rapidly progressing<sup>[5]</sup> and the control over the final geometry and physicochemical properties becomes tighter,<sup>[6]</sup> protein materials are gaining functional and structural versatility as vehicles from chemically coupled drugs. However, many protein species are, themselves, efficient drugs usable in human therapy, as attested by more than 400 protein-based products approved by main medicines agencies.<sup>[7]</sup> Therefore, it would be interesting to test if recombinant

N. Serna, L. Sánchez-García, Dr. N. Ferrer-Miralles, Dr. E. Vázquez, Prof. A. Villaverde  
Institut de Biotecnologia i de Biomedicina  
Universitat Autònoma de Barcelona  
Bellaterra 08193, Barcelona, Spain  
E-mail: antoni.villaverde@uab.cat


N. Serna, L. Sánchez-García, Dr. N. Ferrer-Miralles, Dr. E. Vázquez, Prof. A. Villaverde  
Departament de Genètica i de Microbiologia  
Universitat Autònoma de Barcelona  
Bellaterra 08193, Barcelona, Spain

N. Serna, Dr. M. V. Céspedes, L. Sánchez-García, Dr. U. Unzueta, R. Sala, Dr. N. Ferrer-Miralles, Prof. R. Mangues, Dr. E. Vázquez, Prof. A. Villaverde  
CIBER de Bioingeniería  
Biomateriales y Nanomedicina (CIBER-BBN)  
Bellaterra 08193, Barcelona, Spain  
E-mail: RMangues@santpau.cat

Dr. M. V. Céspedes, Dr. U. Unzueta, R. Sala, Prof. R. Mangues  
Biomedical Research Institute Sant Pau (IIB-Sant Pau)  
and Josep Carreras Research Institute  
Hospital de la Santa Creu i Sant Pau  
08025 Barcelona, Spain

Dr. A. Sánchez-Chardi  
Servei de Microscòpia  
Universitat Autònoma de Barcelona  
Bellaterra 08193, Barcelona, Spain

F. Cortés  
Servei de Cultius Cel·lulars  
Producció d'Anticossos i Citometria  
Universitat Autònoma de Barcelona  
Bellaterra 08193, Barcelona, Spain

 The ORCID identification number(s) for the author(s) of this article can be found under <https://doi.org/10.1002/adfm.201700919>.

DOI: 10.1002/adfm.201700919

protein drugs might be engineered as self-organizing building blocks of functional nanoparticles, which in this form, would exhibit intrinsic therapeutic activities. This might allow excluding the need of further activation and drug conjugation, as the nanomaterial itself would act as a nanoscale drug (desirably between 8 and 100 nm). In this way, chemically homogenous protein nanoparticles with intrinsic therapeutic activities (like the current plain protein species used in human medicine, -e.g., hormones, growth factors, vaccines, etc.) could be biologically produced in a single step as nanoscale assembled oligomers. Acting the material itself as a drug, the possibility of drug leakage during circulation would be largely minimized, especially for proteolytically stable polypeptides. Because of the easy protein engineering, building blocks might also contain functional peptides such as cell-targeting agents, endosomolytic agents or nuclear localization signals, in the form of fused stretches with modular organization. To explore this innovative concept, we have applied a nanoarchitectonic principle based on the addition, to a core protein, of a cationic N-terminal domain plus a C-terminal polyhistidine.<sup>[8]</sup> It is known that these end-terminal tags and the resulting charge distribution in the whole fusion promote self-assembling and oligomerization of monomeric proteins as robust toroid nanoparticles, stable in plasma<sup>[9]</sup> and with high cellular penetrability if empowered with cell-targeting peptides.<sup>[10]</sup> By using this strategy, we have demonstrated here the possibility to generate multifunctional nanoscale materials that being chemically homogenous, act simultaneously as drugs and targeting agents. This proof-of-concept opens a plethora a new therapeutic opportunities based on protein-only supramolecular materials with intrinsic functionalities. These entities can be easily produced by the same biological procedures used during more than 30 years for conventional, unassembled protein pharmaceuticals.

## 2. Results and Discussion

It is known that cationic and histidine-rich end-terminal promote self-assembling and oligomerization of monomeric proteins as robust toroid nanoparticles, stable in plasma and with high cellular penetrability if empowered with cell-targeting peptides.<sup>[9]</sup> We tested if this principle could be applied to therapeutic proteins by engineering the functional BH3 domain of the proapoptotic Bcl-2 homologous antagonist killer (BAK) protein. We aimed to convert it in the building block of self-assembling protein-only nanoparticles with intrinsic antitumoral activities. BAK is a well-known pro-apoptotic factor belonging to the Bcl-2 protein family that triggers programmed cell death by caspase-dependent apoptotic pathway through inactivating antiapoptotic proteins, permeabilizing the mitochondrial membrane, and consequently, releasing cytochrome C and other mitochondrial cell death factors.<sup>[11,12]</sup> Although the full length BAK is reluctant to biological fabrication (because of its highly hydrophobic nature linked to the transmembrane region), truncated forms containing the functional BH3 domain exert proapoptotic activities.<sup>[13]</sup> Of course, whether BH3 BAK would be still functional as assembled into cell-targeted nanoparticles could not be predicted in advance.

To explore this possibility, we fused the cationic peptide T22, a potent CXCR4-ligand that targets metastatic CXCR4<sup>+</sup> colorectal cancer stem cells in vivo,<sup>[9]</sup> to the BAK BH3 domain, for the construction of a BAK-based building block (Figure 1A). The green fluorescent protein (GFP) was incorporated to the fusion platform to conveniently monitor the localization of the material and to explore the potential use of the material in diagnosis as well as in therapy (or for theragnosis).<sup>[14]</sup> The chimeric protein was biofabricated in *Escherichia coli* (*E. coli*) and purified by conventional procedures in form of a unique and stable molecular species with the expected mass (Figure 1B). As expected, the protein spontaneously assembled into discrete, monodisperse materials of about 13.5 nm in diameter, which upon treatment with sodium dodecyl sulfate (SDS) disassembled into building blocks of >7 nm (Figure 1C). T22-BAK-GFP-H6 monomers were slightly larger than BAK-GFP-H6 protein (<7 nm), that remained unassembled because of the absence of the cationic T22. Disassembling was not observed upon 5 h incubation in Optipro complex culture medium (not shown), indicative of stability of nanoparticles in complex physiological media. Also, T22-BAK-GFP-H6 nanoparticles were fluorescent, exhibiting a specific green fluorescence emission of  $306.7 \pm 7.8$  units  $\mu\text{g}^{-1}$ , appropriate for quantitative imaging. High-resolution scanning electron microscopy revealed these materials as planar objects with regular morphology (Figure 1D). Regarding functional analyses, we first determined the ability of protein nanoparticles to bind and penetrate, in a receptor-dependent way, CXCR4<sup>+</sup> cells. Indeed, the assembled T22-BAK-GFP-H6 protein efficiently penetrated CXCR4<sup>+</sup> HeLa and SW1417 cells (Figure 2A). The kinetics of accumulation was compatible with receptor-mediated endocytosis (Figure 2B), while the uptake was CXCR4-dependent, as the inhibitor of T22-CXCR4 interaction, AMD3100,<sup>[15]</sup> dramatically reduced the intracellular fluorescence in both cell lines upon exposure. The control T22-devoid construct failed to enter cells (Figure 2C). The efficient penetration of T22-BAK-GFP-H6 was confirmed by the generic occurrence of fluorescence in most exposed cells (Figure 2D), and by the intracellular accumulation of the material in the perinuclear region (Figure 2E). T22-BAK-GFP-H6 was intrinsically nontoxic, as the viability of CXCR4<sup>+</sup> cells, into which the materials do not penetrate, remained unaltered after prolonged exposure (Figure 2B, inset).

Given the high CXCR4-linked cell penetrability of T22-BAK-GFP-H6 nanoparticles we tested the new material in a mouse model of CXCR4<sup>+</sup> colorectal cancer, regarding biodistribution and capacity of the material to induce selective apoptosis in tumoral tissues. The systemic administration of T22-BAK-GFP-H6 nanoparticles through the tail vein resulted in a transient accumulation of the material in tumor, peaking at 5 h as determined by ex vivo fluorescence images and by IHC (Figure 3A–C). Other relevant organs such as kidney showed only residual fluorescence emission levels (Figure 3D), confirming not only the desired localization of the materials but also the absence of significant renal accumulation, aggregation in lung or detectable toxicity in the time-course (Figure 3D,E). In particular, the absence of protein in kidney (Figure 3D,F) was fully indicative of a high stability of the oligomers in plasma, as monomeric or disassembled proteins, even when targeted to specific tumoral markers by tumor-homing peptides,



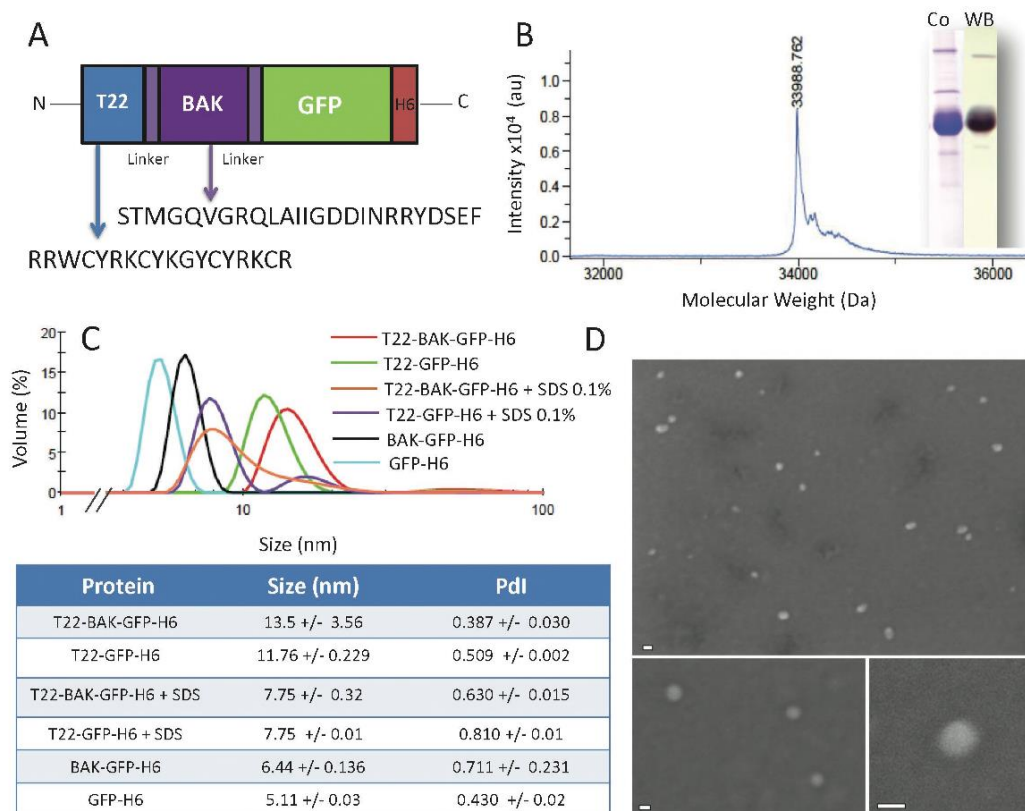


**Figure 1.** Design and biochemical characterization of T22-BAK-GFP-H6 nanoparticles. A) Schematic representation of the CXCR4-binding T22-BAK-GFP-H6 building block indicating its modular composition. The amino acid sequences of the CXCR4 peptide ligand T22 and the therapeutic BH3 domain of BAK protein are shown. Lengths of the modules are approximate. The linker sequence is GGSSRSSS. B) Mass spectrometry of the purified T22-BAK-GFP-H6 fusion indicating the experimental molecular weight (33 988.762 Da). Protein integrity is also shown through Coomassie blue-stained sodium dodecyl sulfate polyacrylamide gel electrophoresis gels (Co) and by H6 immunodetection in Western blot (WB). C) Hydrodynamic size distribution of T22-empowered nanoparticles in their native state and upon SDS-mediated disassembling. The parental BAK-GFP-H6 and GFP-H6 proteins that do not assemble and the related T22-GFP-H6 particles (and SDS-mediated disassembled monomers) are included here for size comparison. All proteins were in solution in their respective storage buffers. D) FESEM images of randomly selected fields showing the ultrastructural morphology of T22-BAK-GFP-H6 nanoparticles. Bars indicate 20 nm.

accumulate in kidney.<sup>[9]</sup> At 24 but not at 48 h, the tumor still showed detectable fluorescence (Figure 3B), indicating prolonged permanence of nanoparticles in the target organ.

As compared to the parental T22-GFP-H6 or the untargeted BAK-GFP-H6 protein, T22-BAK-GFP-H6 induced a significantly decrease of mitotic figures (Figure 4A), that must be consequently attributed to the targeted penetration of functional BAK. This was associated with caspase-3 activation, proteolysis of PARP, occurrence of apoptotic bodies and increased necrotic areas in tumor tissues shortly (2 h) after the administration of the treatment in mice (Figure 4B–F). Tumor cell apoptosis peaked at 5 h and it was maintained for at least 48 h (Figure 4A). By contrast, the nontargeted BAK-GFP-H6 protein yielded only a negligible level of caspase-3 activation or apoptosis in tumors, since it did not differ from the background in buffer-treated tumors (Figure 4F). Histological alterations were not observed in any of the explored nontarget organs (Figure 3E). These observations proved not only the molecular availability of the BAK BH3 domain when delivered as regular

nanoparticles but, as envisaged, that T22-BAK-GFP-H6 nanoparticles exhibited intrinsic biological activity.

At this stage, we wondered how much generic applicability the platform based on therapeutic protein-only nanoparticles would have. In principle, any recombinant protein should be suitable for being empowered as building blocks of functional nanoparticles. In this context, we tested the formation of functional nanoscale materials based on the p53-upregulated modulator of apoptosis PUMA<sup>[16]</sup> and the antimicrobial peptide GWH1,<sup>[17]</sup> both also inducing apoptosis upon internalization in cancer cells. Under the same modular scheme than T22-BAK-GFP-H6, T22-PUMA-GFP-H6 (Figure 5A), and T22-GWH1-GFP-H6 (Figure 5B) form nanoparticles of 20 and 24 nm, respectively, that as in the case of BAK-based construct retain the GFP fluorescence (not shown). When administered in vivo, both nanoparticles accumulate in tumor (Figure 5C,D), with a minor occurrence of T22-GWH1-GFP-H6 in kidney. This is again indicative of the stability of the oligomers in plasma as materials over 8 nm in size, what prevents renal filtration.<sup>[9]</sup>



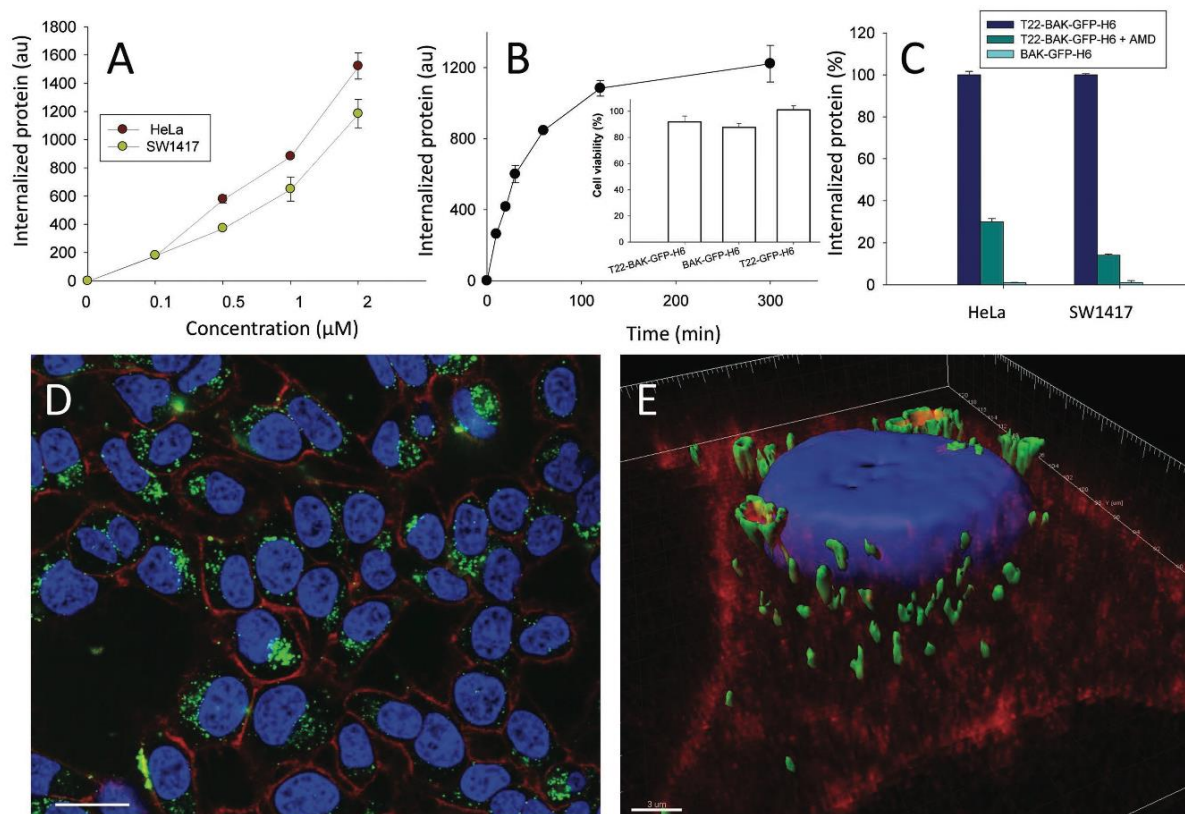


**Figure 2.** Cell penetrability of T22-BAK-GFP-H6 nanoparticles. A) Internalization of T22-BAK-GFP-H6 nanoparticles in cultured CXCR4<sup>+</sup> HeLa and SW1417 cells after 24 h exposure. The intensity of intracellular fluorescence is corrected by specific fluorescence, resulting into arbitrary units (au) that are representative of protein amounts. B) Time-dependent intracellular accumulation of nanoparticles ( $2 \times 10^{-6}$  M) by HeLa cells. Inset: viability of CXCR4<sup>+</sup> SW1417 cells upon exposure to  $2 \times 10^{-6}$  M T22-BAK-GFP-H6 nanoparticles for 48 h. C) Specificity of CXCR4-mediated internalization of T22-BAK-GFP-H6 nanoparticles determined by the use of the CXCR4<sup>+</sup> inhibitor AMD3100. D) Intracellular localization of T22-BAK-GFP-H6 nanoparticles upon 24 h of exposure to HeLa cells, observed by confocal sections. Nanoparticles are seen in green since they are naturally fluorescent, while nuclei are labeled in blue and cell membranes in red. Bar indicates 25  $\mu$ m. E) Details of targeted cells during the uptake of nanoparticles in a 3D confocal reconstruction. Bar indicates 3  $\mu$ m.

Both type of nanoparticles significantly reduced the mitotic rates and even with some variability, the drug materials tended to induce cell death and promote selective necrosis in tumoral tissues, this effect being significant in the case of the PUMA-based material (Figure 5E,F).

Taking all these data together, we have here demonstrated that three different proapoptotic proteins, engineered to self-assemble as nanoscale protein materials, act themselves as chemically homogenous drugs that do not need further activation or functionalization upon production. In this nanoscale form and upon specific receptor-mediated internalization, the core protein stretches of these therapeutic materials, namely, BH3 BAK, PUMA, and GWH1 are available for functionality. It is known that BH3 BAK binds antiapoptotic proteins,<sup>[12]</sup> inhibits them and alters the balance between proapoptotic and antiapoptotic proteins. This, in turn, induces caspase activation and PARP proteolysis without loss of mitochondrial membrane potential or detectable translocation of cytochrome c from mitochondria to cytosol.<sup>[18]</sup> In this regard, we have indeed confirmed the absence of cytochrome C activation in target tissues

(not shown) upon nanoparticle administration. The global effect could be initiated by the interaction between the exposed BH3 motifs in the nanoparticle and the antiapoptotic protein Bcl-XL, which would displace BAK from the BAK/Bcl-XL heterodimers, leading to the oligomerization and retrotranslocation of the free proapoptotic BAK protein to the OMM and apoptosis initiation.<sup>[19]</sup> This argument is supported by previous *in vitro* work demonstrating that BAK overexpression<sup>[20]</sup> or exogenous BH3 BAK peptides antagonize the Bcl-XL function, triggering fast caspase-3 dependent apoptosis in tumor cells.<sup>[13]</sup> By contrast, the induction of intrinsic (mitochondrial-mediated) apoptosis by genotoxic drugs (e.g., in chemotherapy) requires at least 24 h to be completed,<sup>[21,22]</sup> because of the time interval required upon DNA damage check point activation to reach the cellular decision between DNA repair and induction of cell death.<sup>[23]</sup>

Similarly, PUMA is a (Bcl-2 homology 3) BH3-only protein that triggers cell death by interacting with pro and antiapoptotic proteins of the Bcl-2 family.<sup>[24]</sup> This protein directly activates BAX and BAK,<sup>[24,25]</sup> and it also binds to pro-survival proteins

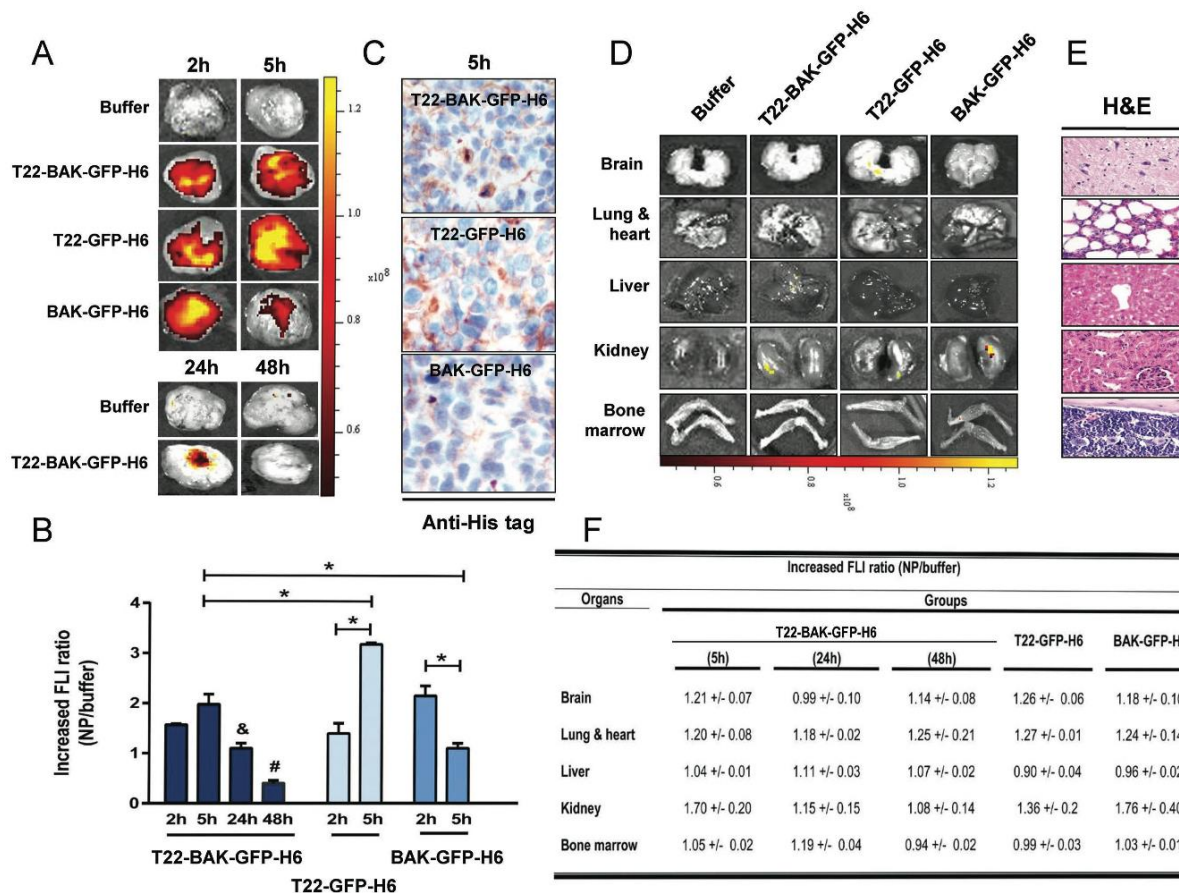


**Figure 3.** Accumulation and organ biodistribution of T22-GFP-H6 and T22-BAK-GFP-H6 nanoparticles and unassembled BAK-GFP-H6 protein in CXCR4<sup>+</sup> colorectal tumors. A) Representative ex vivo tumor fluorescence images (FLI) at 2, 5, 24, and 48 h after iv administration of 330  $\mu\text{g}$  dose of each protein. B) GFP fluorescence quantitation in tumors at 2, 5, 24, and 48 h using the IVIS spectrum system. The FLI ratio was calculated dividing the GFP signal from the protein-treated mice by the autofluorescent signal of buffer-treated mice at each organ. & and #  $p < 0.05$  bars indicate statistically significant compared to the rest of T22-BAK-GFP-H6-treated groups. \* $p < 0.05$  bars indicate a statistically significant between the designated groups. C) Immunohistochemistry against the His-tag domain of the nanoparticles in the tumors at 5 h. D) Representative ex vivo images of the material accumulated in mouse brain, lung, heart, liver, kidney, and bone marrow tissues after treatment. Note the absence or residual fluorescence in these organs compared to tumors. E) Representative H&E staining showed no altered architecture in any organ. F) Quantitation of GFP fluorescence signal in brain, lung and heart, liver, kidney, and bone marrow tissues expressed as fluorescence ratio. This was calculated by dividing the fluorescence of each organ in protein-treated mice by the autofluorescence measured in buffer-treated mice of the respective organ of the time-course experiment. The fluorescence of all protein doses (334  $\mu\text{g}$  each) was recorded by IVIS (total radiant efficiency) just before administration (T22-GFP-H6:  $8.4 \times 10^{11}$  [ $\text{p s}^{-1}$ ]/ $[\mu\text{W cm}^{-2}]$ ; T22-BAK-GFP-H6:  $8.1 \times 10^{11}$  [ $\text{p s}^{-1}$ ]/ $[\mu\text{W cm}^{-2}]$ ; BAK-GFP-H6:  $8.5 \times 10^{11}$  [ $\text{p s}^{-1}$ ]/ $[\mu\text{W cm}^{-2}]$ ) and the final generated data were corrected by specific fluorescence to allow precise comparison between materials and time points. Data expressed as mean  $\pm$  SE. Abbreviations: H&E, hematoxylin and eosin staining; iv: intravenous; FLI: fluorescent imaging; NP: nanoparticle.

(Bcl-2 and Bcl-XL) through the BH3 domain<sup>[26]</sup> acting as a decoy and preventing their binding and therefore the inhibition of BAX and BAK. On the other hand, GWH1 exerts its cytolytic activity by folding into an amphipathic helix,<sup>[17]</sup> which is probably conserved in T22-GWH1-GFP-H6. Although showing a milder effect than the other tested constructs, GWH1 in form of nanomaterial is supposed to exert cell lytic effects by two sequential events consisting on binding to cell membranes followed by permeabilization.

In the context of the pushing needs of cell-targeting and of biocompatible materials as nanoscale drug vehicles, engineering therapeutic proteins into protein-only nanoparticles with

intrinsic therapeutic activity represents a totally new concept of immediate transversal applicability. In contrast to conventional heterogeneous nanoconjugates, in which nonprotein carriers are chemically functionalized for drug loading,<sup>[27]</sup> self-assembling protein drugs are produced in form of nanoparticles in a single step by biological fabrication.<sup>[28]</sup> This approach allows avoiding the risk of drug leakage during circulation and prevents any potential toxicity associated to some of the materials used as nanoscale drug vehicles. Protein plasticity further allows the generation of modular constructs in which diverse functions such as cell targeting and even fluorescence emission can be combined with the therapeutic protein itself, without increasing



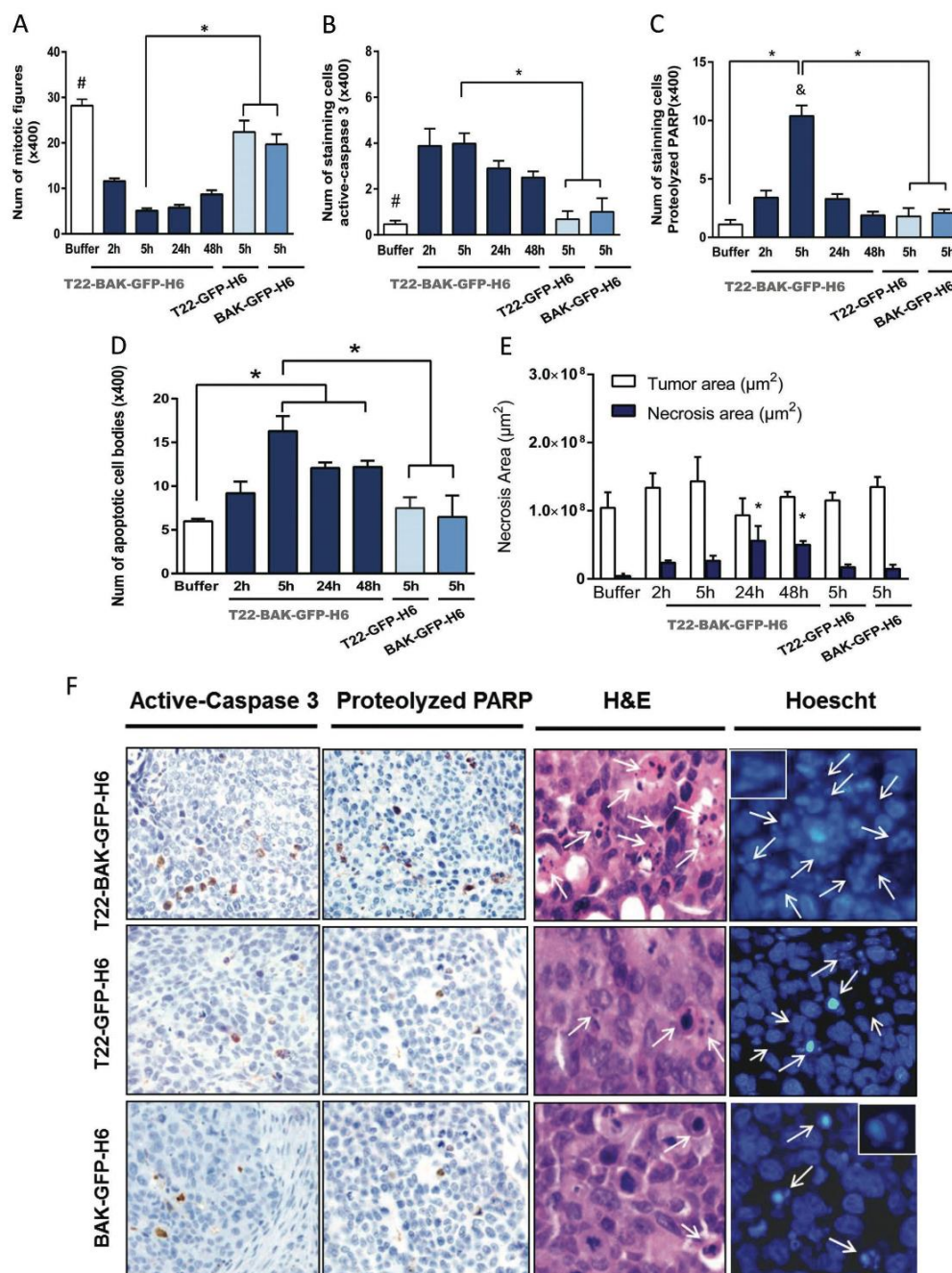


**Figure 4.** Reduced proliferation index, caspase-3 activation, proteolyzed PARP, apoptosis induction, and necrotic rates in tumors bearing mice at 2, 5, 24, and 48 h after administration of T22-BAK-GFP-H6 compared to buffer and T22-GFP-H6 and BAK-GFP-H6 control counterparts. Quantitation in tumors of the number of mitotic figures (mitotic activity index) by A) H&E staining and both, B) cleaved (active) caspase-3 and C) proteolyzed PARP positive tumor cells by IHC. #, &  $p < 0.05$  bars indicate statistically significant compared to T22-BAK-GFP-H6-treated groups at each time; \* $p < 0.05$  bars indicate statistically significant between the designated groups. D) Counts of apoptotic figures detected by nuclear condensation after Hoechst staining. \* $p < 0.05$  bars indicate statistically significant between the designated groups. E) Measurements of total and necrotic area ( $\mu\text{m}^2$ ) in low-power field magnification tumor slices using the Cell D software. \* $p < 0.05$  bars indicate statistically significant between 2 and 5 h treated groups. F) Representative microphotographs of active caspase-3 and proteolyzed PARP positive cells (stained tumor cells), and cell dead bodies by both, H&E, and Hoechst staining (white arrows) 5 h after treatment with T22-BAK-GFP-H6 and control counterpart nanoparticles ( $\times 400$  magnification; inserts at  $\times 1000$  magnification). All quantified values in panels (A–D) were obtained by counting 10 high-power field ( $\times 400$ ) per sample. Data were expressed as mean  $\pm$  SE. All statistical analyses were performed applying the Mann Whitney U-test. Abbreviations: H&E, hematoxylin and eosin staining.

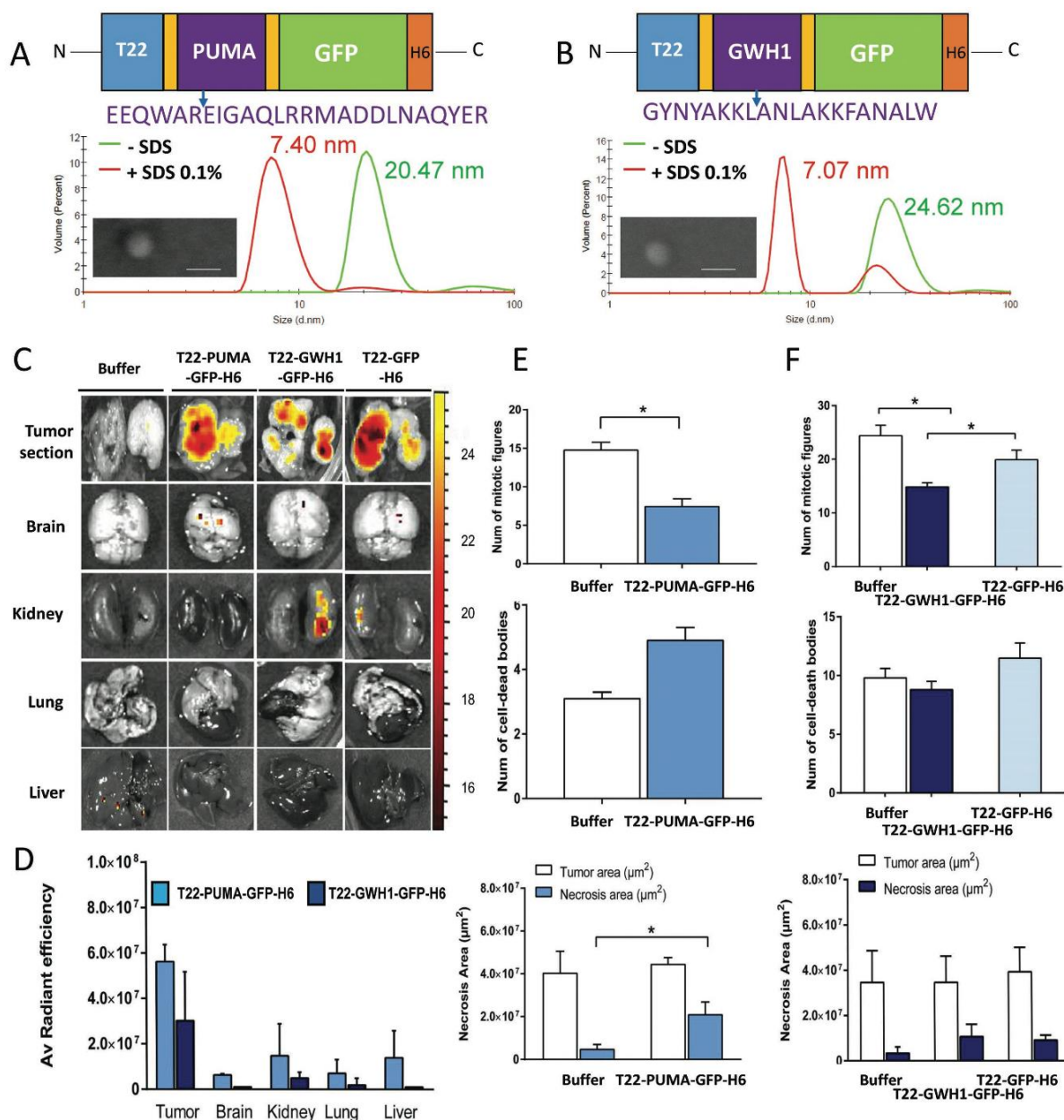


**Figure 5.** Physical and biological characterization of T22-PUMA-GFP-H6 and T22-GWH1-GFP-H6 nanoparticles. Schematic representation of the building blocks based on A) PUMA and on B) GWH1. The amino acid sequences of the therapeutic protein stretches are indicated while the rest of the constructs are as in Figure 1. The DLS plots of the nanoparticles (green) and of the disassembled building blocks (red) are depicted, sided by the value of the peaks in nm. Representative FESEM images of isolated nanoparticles are also shown. Bars indicate 40 nm. C) Representative ex vivo tumor fluorescence images (FLI) and normal organs (brain, kidney, lung, heart, and liver tissues) after iv administration of 330  $\mu\text{g}$  dose of each nanoparticle at 5 h. D) Quantitation of fluorescence signal (radiant efficiency) in the respective organs. E,F) Quantitation of the number of mitotic figures, (H&E staining), the number of apoptotic figures detected by nuclear condensation after Hoechst staining and necrosis area (H&E staining) in tumors at 5 after the administration of T22-PUMA-GFP-H6 or T22-GWH1-GFP-H6 compared to T22-GFP-H6 control counterpart. All quantitations were done as indicated in Figure 4. The fluorescence of protein doses recorded by IVIS just before the administration were  $8.9 \times 10^{11}$  [ $\text{p s}^{-1}$ ]/ $[\mu\text{W cm}^{-2}]$  (T22-PUMA-GFP-H6) and  $7.4 \times 10^{11}$  [ $\text{p s}^{-1}$ ]/ $[\mu\text{W cm}^{-2}]$  (T22-GWH1-GFP-H6), respectively, and generated data were adjusted for comparisons as indicated in Figure 3.

the complexity of the production process (that remains restricted to a single recombinant polypeptide). The self-assembling platform based on cationic end-terminal peptides is universal and

performs irrespective of the nature of the core polypeptide,<sup>[29]</sup> allowing its application in a theoretically unlimited catalogue of therapeutic proteins. If having a human origin, the resulting



constructs should not pose immunogenicity limitations in repeated administrations, which are only observed in the case of live-lasting chronic diseases that require live-lasting repeated doses (such as rare diseases). For that, and although GFP has been successfully incorporated in the prototypes presented here as a convenient reporter for cell internalization and systemic biodistribution, GFP-free human proteins would be highly desirable as final drugs. Also, the convenient size of the constructs between  $\approx 8$  and 100 nm prevents renal filtration and aggregation and favors cell internalization, what is also enhanced by the multivalent display of the homing peptide.<sup>[6]</sup>

The presented approach, illustrated here with three structurally unrelated tumor-targeted proapoptotic factors in a colorectal cancer model, shall be transversally explored for the further development of self-assembling, self-delivered homogeneous materials for the increasing number of human pathologies recognized as systemically treatable with protein drugs.

### 3. Experimental Section

**Protein Design, Production, and Purification:** The engineered fusion proteins were named according to their modular organization (Figures 1 and 5). Synthetic genes were designed in house and obtained from GeneArt inserted into the prokaryotic expression pET-22b vector. The encoded proteins were produced in plasmid-bearing *E. coli Origami B* (BL21, OmpT<sup>-</sup>, Lon<sup>-</sup>, TrxB<sup>-</sup>, Gor<sup>-</sup>, Novagen) cells, cultured in 2 L-shaker flasks with 500 mL of LB medium with 100  $\mu\text{g mL}^{-1}$  ampicillin, 15  $\mu\text{g mL}^{-1}$  kanamycin, and 12.5  $\mu\text{g mL}^{-1}$  tetracycline at 37 °C. Recombinant gene expression was induced at an OD<sub>550</sub> around 0.5–0.7 upon the addition of  $0.1 \times 10^{-3}$  M isopropyl- $\beta$ -D-thiogalactopyranoside and then, bacterial cells were kept growing 3 h at 37 °C for T22-BAK-GFP-H6 production and overnight at 20 °C for T22-GFP-H6, T22-GWH1-GFP-H6, and T22-PUMA-GFP-H6 production. Bacterial cells were then harvested by centrifugation at 5000 g for 15 min at 4 °C and resuspended in wash buffer (20  $\times 10^{-3}$  M Tris-HCl, 500  $\times 10^{-3}$  M NaCl, 10  $\times 10^{-3}$  M imidazol, pH 8.0) in the presence of EDTA-free protease inhibitor (Complete EDTA-Free; Roche, Basel, Switzerland). Cells were disrupted at 1200 psi in a French Press (Thermo FA-078A) and lysates were centrifuged for 45 min (15 000 g at 4 °C). All proteins were purified by His-tag affinity chromatography using HiTrap Chelating HP 1 mL columns (GE Healthcare, Piscataway, NJ, USA) by AKTA purifier FPLC (GE Healthcare). After filtering the soluble fraction, samples were loaded onto the column and washed with 10 column volumes of wash buffer. Elution was achieved by a linear gradient of 20  $\times 10^{-3}$  M Tris-HCl, 500  $\times 10^{-3}$  M NaCl, 500  $\times 10^{-3}$  M imidazole, pH 8.0, and purified fractions were collected and analyzed by SDS-PAGE and Western Blotting with anti-His monoclonal antibody (Santa Cruz Biotechnology, Heidelberg, Germany) to observe the protein of interest. Proteins were dialyzed overnight at 4 °C, against sodium bicarbonate buffer with salt (166  $\times 10^{-3}$  M NaHCO<sub>3</sub>, pH 7.4 + 333  $\times 10^{-3}$  M NaCl). These buffers were the final solvents for further experiments. Protein integrity and purity were checked by mass spectrometry (MALDI-TOF) and quantified by Bradford's assay.

**Fluorescence Determination, Dynamic Light Scattering (DLS), and Field Emission Scanning Electron Microscopy (FESEM):** The fluorescence of the fusion proteins was determined in a Varian Cary Eclipse fluorescence spectrophotometer (Agilent Technologies, Palo Alto, CA, USA) at 510 nm using an excitation wavelength of 450 nm. Volume size distribution of nanoparticles and monomeric GFP protein fusions were determined by DLS at 633 nm (Zetasizer Nano ZS, Malvern Instruments Limited, Malvern, UK). For fluorescence determination, protein samples were diluted in the corresponding storage buffer to 0.5 mg mL<sup>-1</sup>, in 100  $\mu\text{L}$  final volume. For DLS analyses, proteins (stored at  $-80$  °C) were thawed and 50  $\mu\text{L}$  of each sample was used. FESEM qualitative analyses were performed with Zeiss Merlin (Zeiss, Oberkochen, Germany) field

emission scanning electron microscope operating at 1 kV and equipped with a high resolution in-lens secondary electron detector. Microdrops of diluted purified proteins were deposited onto silicon wafer surfaces (Ted Pella, Reading, CA, USA), air-dried, and immediately observed.

**Cell Culture and Flow Cytometry:** The CXCR4<sup>+</sup> HeLa cell line (ATCC-CCL-2) was cultured in Eagle's minimum essential medium (Gibco, Rockville, MD, USA) supplemented with 10% fetal calf serum (Gibco), and incubated at 37 °C and 5% CO<sub>2</sub> in a humidified atmosphere. Meanwhile SW1417 cell line was maintained in Dulbecco's modified Eagle's medium (Gibco GlutaMAX, Thermo Fisher Scientific, Waltham, MA, USA) supplemented with 10% fetal calf serum (Gibco), and incubated at 37 °C and 10% CO<sub>2</sub> in a humidified atmosphere. HeLa and SW1417 cell lines were cultured on 24-well plate at  $3 \times 10^4$  and  $12 \times 10^4$  cells per well respectively for 24 h until reaching 70% confluence. Nanoparticles and monomeric proteins were added at different concentrations (ranging from  $0.1 \times 10^{-6}$  to  $2 \times 10^{-6}$  M) to the cell culture in the presence of Optipro medium (Gibco) 24 h before the flow cytometry analysis. Cell samples were analyzed on a FACSCanto system (Becton Dickinson, Franklin Lakes, NJ, USA) using a 15 W air-cooled argon-ion laser at 488 nm excitation. GFP fluorescence emission was measured with a detector D (530/30 nm band pass filter) after an adapted treatment with 1 mg mL<sup>-1</sup> trypsin (Gibco) for 15 min that ensures the removal of externally attached protein.<sup>[30]</sup> Specific internalization of nanoparticles was measured using AMD3100/CXCR4<sup>+</sup> inhibitor (octahydrochloride hydrate, Sigma-Aldrich, Steinheim, Germany). For this experiment, T22-BAK-GFP-H6 was labeled with ATTO488 (41698, Sigma-Aldrich) during 1 h in darkness at room temperature to obtain a more fluorescent protein. T22-BAK-GFP-H6-ATTO488 was added at  $25 \times 10^{-9}$  M during 1 h of incubation in presence of AMD3100 at 1:10 ratio.

**Confocal Microscopy:** HeLa cells were grown on Mat-Tek culture dishes (MatTek Corporation, Ashland, MA, USA). Medium was removed and cells were washed with DPBS, OptiPro medium supplemented with L-glutamine and proteins were added 24 h before staining at  $2 \times 10^{-6}$  M. Nuclei were labeled with 0.2  $\mu\text{g mL}^{-1}$  Hoechst 33342 (Molecular Probes, Eugene, OR, USA) and the plasma membranes with 2.5  $\mu\text{g mL}^{-1}$  CellMask Deep Red (Molecular Probes) in darkness for 10 min. Live cells were recorded by TCS-SP5 confocal laser scanning microscopy (Leica Microsystems, Heidelberg, Germany) using a Plan Apo 63  $\times$ /1.4 (oil HC  $\times$  PL APO lambda blue) objective. To determine the location of particles inside the cell, stacks of 10–20 sections were collected at 0.5  $\mu\text{m}$  Z-intervals with a pinhole setting of 1 Airy unit. Images were processed and the 3D reconstruction was generated using Imaris version 7.2.1.0 software (Bitplane, Zürich, Switzerland).

**Biodistribution:** Five-week-old female Swiss nu/nu mice weighing between 18 and 20 g (Charles River, L'Abresle, France) and maintained in specific-pathogen-free (SPF) conditions, were used for in vivo studies. All the in vivo procedures were approved by the Hospital de Sant Pau Animal Ethics Committee and performed according to European Council directives. To generate the subcutaneous mouse model, 10 mg of SP5 CCR tumor tissue was obtained from donor animals and implanted subcutaneously in the subcutis of swiss nu/nu mice. When tumors reached 500 mm<sup>3</sup> approximately, mice were randomly allocated and administered with T22-BAK-GFP-H6, BAK-GFP-H6, and T22-GFP-H6 nanoparticles at 330  $\mu\text{g}$  per mouse dose.

Short (2 and 5 h) and long times (24 and 48 h) were assayed to explore the biological effects of the administered nanoparticles. For that, mice were euthanized and tumor and brain, pancreas, lung and heart, kidney, liver, and bone marrow were collected and examined separately for ex vivo GFP fluorescence in an IVIS Spectrum equipment (PerkinElmer Inc, Waltham, MA, USA). The fluorescent signal (FLI) was first digitalized, displayed as a pseudocolor overlay, and expressed as radiant efficiency. The FLI ratio was calculated dividing the FLI signal from the protein-treated mice by the FLI autofluorescent signal of control mice. Finally, all organs were collected and fixed with 4% formaldehyde in phosphate-buffered solution for 24 h. These samples were then embedded in paraffin for histological and immunohistochemical analyses as well as for determination of mitotic and apoptotic index and necrosis evaluation.

**Histopathology and Immunohistochemistry Analyses:** 4  $\mu\text{m}$  thick sections were stained with hematoxylin and eosin (H&E), and a complete histopathological analysis was performed by two independent observers. The presence and location of the His tag in the protein materials and of the proteolyzed Poly (ADP-Ribose) polymerase (PARP) and the active cleaved-Caspase 3 protein in tissue sections were assessed by immunohistochemistry using the DAKO immunosystem equipment and standard protocols. A primary antibody against the His tag (1:1000; MBL International, Woburn, MA, USA), anti-PARP p85 fragment pAb (1:300; Promega, Madison, WI, USA) or antiactive caspase 3 antibody (1:300, BD PharMingen, San Diego, CA, USA) were incubated for 25 min after incubation with the secondary antibody in tumor tissues at 2, 5, 24, and 48 h. The number of stained cells was quantified by two independent blinded counters who recorded the number of positive cells per 10 high-power fields (magnification 400 $\times$ ). Representative pictures were taken using Cell $\Delta$ B software (Olympus Soft Imaging v 3.3, Nagano, Japan).

**Assessment of Mitotic, Apoptotic, Necrotic Rates:** Tumor slices were also processed to assess proliferation capacity by counting the number of mitotic figures per ten high-power fields (magnification  $\times$ 400) in H&E stained tumors. Apoptotic induction was evaluated by the presence of cell death bodies in H&E and also by Hoechst staining in tumor slices. Hoechst 33258 (Sigma-Aldrich, Steinheim, Germany) staining was performed in Triton X-100 (0.5%) permeabilized sections. Slides were then stained with Hoechst 33258 (1:5000 in PBS) for 1 h, rinsed with water, mounted, and analyzed under fluorescence microscope ( $\lambda_{\text{ex}} = 334 \text{ nm}$ / $\lambda_{\text{em}} = 465 \text{ nm}$ ). The number of apoptotic bodies was quantified by two independent blinded recording the number of condensed and/or defragmented nuclei per 10 high-power fields (magnification 400 $\times$ ). Necrosis area in tumors was quantified using Cell $\Delta$ B software at 15 $\times$  magnification and representative pictures were taken using the same Cell $\Delta$ B software at 400 $\times$  magnification.

## Acknowledgements

N.S. and M.V.C. contributed equally to this work. The authors are indebted to MINECO (BIO2013-41019-P), AGAUR (2014SGR-132), and CIBER de Bioingeniería, Biomateriales y Nanomedicina (Project NANOPROTHER) to A.V., Marató de TV3 foundation (TV32013-3930) and FIS (PI15/00272, cofunding ISCIII and FEDER) to E.V., and ISCIII (PI15/00378 and PIE15/00028, cofunding FEDER), Marató TV3 (2013-2030), and AGAUR2014-PROD0005 to R.M. for funding the research on protein-based therapeutics. Protein production was performed in part by the ICTS "NANBIOSIS," more specifically by the Protein Production Platform of CIBER in Bioengineering, Biomaterials & Nanomedicine (CIBER-BBN)/IBB, at the UAB SepBioES scientific-technical service (<http://www.nanbiosis.es/unit/u1-protein-production-platform-ppp/>). All in vivo experiments were performed by the ICTS "NANBIOSIS," more specifically by the CIBER-BBN's Nanotoxicology Unit Platform. A.V. received an ICREA ACADEMIA award. M.V.C. was supported by a Miguel Servet contract and U.U. received a Sara Borrell postdoctoral fellowship, both from ISCIII, while L.S.-G. was supported by AGAUR (FI-DGR).

## Conflict of Interest

MVC, UU, RM, EV and AV are co-inventors in a patent on the uses of T22 as a tumor-targeting agent (WO2012095527).

## Keywords

advanced therapies, nanoparticles, protein materials, self-assembly, therapeutic proteins

Received: February 18, 2017

Revised: May 8, 2017

Published online: July 4, 2017

- [1] R. Duncan, R. Gaspar, *Mol. Pharm.* **2011**, *8*, 2101.
- [2] D. Peer, J. M. Karp, S. Hong, O. C. Farokhzad, R. Margalit, R. Langer, *Nat. Nanotechnol.* **2007**, *2*, 751.
- [3] B. Feng, J. L. LaPerle, G. Chang, M. V. Varma, *Expert Opin. Drug Metab. Toxicol.* **2010**, *6*, 939.
- [4] N. Sanvicens, M. P. Marco, *Trends Biotechnol.* **2008**, *26*, 425.
- [5] N. Ferrer-Mirallès, E. Rodríguez-Carmona, J. L. Corchero, E. García-Fruitos, E. Vázquez, A. Villaverde, *Crit. Rev. Biotechnol.* **2015**, *35*, 209.
- [6] U. Unzueta, M. V. Cespedes, E. Vázquez, N. Ferrer-Mirallès, R. Mangués, A. Villaverde, *Trends Biotechnol.* **2015**, *33*, 253.
- [7] L. Sánchez-García, L. Martín, R. Mangués, N. Ferrer-Mirallès, E. Vázquez, A. Villaverde, *Microb. Cell Fact.* **2016**, *15*, 33.
- [8] N. Serna, M. V. Cespedes, P. Saccardo, Z. Xu, U. Unzueta, P. Alamo, M. Pesarrodonna, A. Sánchez-Chardi, M. Roldan, R. Mangués, E. Vázquez, A. Villaverde, N. Ferrer-Mirallès, *Nanomedicine* **2016**, *12*, 1241.
- [9] M. V. Cespedes, U. Unzueta, W. Tatkiwicz, A. Sánchez-Chardi, O. Conchillo-Sole, P. Alamo, Z. Xu, I. Casanova, J. L. Corchero, M. Pesarrodonna, J. Cedano, X. Daura, I. Ratera, J. Veciana, N. Ferrer-Mirallès, E. Vázquez, A. Villaverde, R. Mangués, *ACS Nano* **2014**, *8*, 4166.
- [10] Z. K. Xu, U. Unzueta, M. Roldan, R. Mangués, A. Sánchez-Chardi, N. Ferrer-Mirallès, A. Villaverde, E. Vázquez, *Mater. Lett.* **2015**, *154*, 140.
- [11] F. Llambi, T. Moldoveanu, S. W. Tait, L. Bouchier-Hayes, J. Temirov, L. L. McCormick, C. P. Dillon, D. R. Green, *Mol. Cell* **2011**, *44*, 517.
- [12] D. Westphal, G. Dewson, P. E. Czabotar, R. M. Kluck, *Biochim. Biophys. Acta* **2011**, *1813*, 521.
- [13] E. P. Holinger, T. Chittenden, R. J. Lutz, *J. Biol. Chem.* **1999**, *274*, 13298.
- [14] J. H. Ryu, H. Koo, I. C. Sun, S. H. Yuk, K. Choi, K. Kim, I. C. Kwon, *Adv. Drug Delivery Rev.* **2012**, *64*, 1447.
- [15] U. Unzueta, M. V. Cespedes, N. Ferrer-Mirallès, I. Casanova, J. Cedano, J. L. Corchero, J. Domingo-Espin, A. Villaverde, R. Mangués, E. Vázquez, *Int. J. Nanomed.* **2012**, *7*, 4533.
- [16] Y. Zhang, D. Xing, L. Liu, *Mol. Biol. Cell* **2009**, *20*, 3077.
- [17] Y.-L. Sophia Chen, J.-H. Li, Ch.-Y. Yu, Ch.-J. Lin, P.-H. Chiu, P.-W. Chen, Ch.-Ch. Lin, W.-J. Chen, *Peptides* **2012**, *36*, 257.
- [18] E. P. Holinger, T. Chittenden, R. J. Lutz, *J. Biol. Chem.* **1999**, *274*, 13298.
- [19] F. Todt, Z. Cakir, F. Reichenbach, F. Emschermann, J. Lauterwasser, A. Kaiser, G. Ichim, S. W. Tait, S. Frank, H. F. Langer, F. Edlich, *EMBO J.* **2015**, *34*, 67.
- [20] Q. S. Tong, L. D. Zheng, L. Wang, J. Liu, W. Qian, *BMC Cancer* **2004**, *4*, 33.
- [21] C. Gajate, F. An, F. Mollinedo, *J. Biol. Chem.* **2002**, *277*, 41580.
- [22] D. T. Stefanou, A. Bamias, H. Episkopou, S. A. Kyrtopoulos, M. Likka, T. Kalampokas, S. Photiou, N. Gavalas, P. P. Sfikakis, M. A. Dimopoulos, V. L. Souliotis, *PLoS One* **2015**, *10*, e0117654.
- [23] T. Rich, R. L. Allen, A. H. Wyllie, *Nature* **2000**, *407*, 777.
- [24] E. H. Shroff, C. M. Snyder, G. R. Budinger, M. Jain, T. L. Chew, S. Khuon, H. Perlman, N. S. Chandel, *PLoS One* **2009**, *4*, e5646.
- [25] H. C. Chen, M. Kanai, A. Inoue-Yamauchi, H. C. Tu, Y. Huang, D. Ren, H. Kim, S. Takeda, D. E. Reyna, P. M. Chan, Y. T. Ganesan, C. P. Liao, E. Gavathiotis, J. J. Hsieh, E. H. Cheng, *Nat. Cell Biol.* **2015**, *17*, 1270.
- [26] J. Yu, L. Zhang, P. M. Hwang, K. M. Kinzler, B. Vogelstein, *Mol. Cell* **2001**, *7*, 673.
- [27] E. Vázquez, R. Mangués, A. Villaverde, *Nanomedicine* **2016**, *11*, 1333.
- [28] E. Vázquez, A. Villaverde, *Nanomedicine* **2013**, *8*, 1895.
- [29] U. Unzueta, N. Ferrer-Mirallès, J. Cedano, X. Zikung, M. Pesarrodonna, P. Saccardo, E. García-Fruitos, J. Domingo-Espin, P. Kumar, K. C. Gupta, R. Mangués, A. Villaverde, E. Vázquez, *Bio-materials* **2012**, *33*, 8714.
- [30] J. P. Richard, K. Melikov, E. Vives, C. Ramos, B. Verbeure, M. J. Gait, L. V. Chernomordik, B. Lebleu, *J. Biol. Chem.* **2003**, *278*, 585.

